Katagiri T, Suda T, Miyazono K. 2008. The bone morphogenetic proteins. New York: Cold Spring Harbor Press.

Katagiri T, Yamaguchi A, Komaki M, Abe E, Takahashi N, Ikeda T, Rosen V, Wozney JM, Fujisawa-Sehara A, Suda T. 1994. Bone morphogenetic protein-2 converts the differentiation pathway of C2C12 myoblasts into the osteoblast lineage. J Cell Biol 127:1755–1766.

Katagiri T. 2010. Heterotopic bone formation induced by bone morphogenetic protein signaling: Fibrodysplasia ossificans progressiva. J Oral Biosci 52:33–41.

Knockaert M, Sapkota G, Alarcon C, Massague J, Brivanlou AH. 2006. Unique players in the BMP pathway: Small C-terminal domain phosphatases dephosphorylate Smad1 to attenuate BMP signaling. Proc Natl Acad Sci USA 103:11940–11945.

Kodaira K, Imada M, Goto M, Tomoyasu A, Fukuda T, Kamijo R, Suda T, Higashio K, Katagiri T. 2006. Purification and identification of a BMP-like factor from bovine serum. Biochem Biophys Res Commun 345:1224–1231.

Kokabu S, Ohte S, Sasanuma H, Shin M, Yoneyama K, Murata E, Kanomata K, Nojima J, Ono Y, Yoda T, Fukuda T, Katagiri T. 2011. Suppression of BMP-Smad signaling axis-induced osteoblastic differentiation by small C-terminal domain phosphatase 1, a Smad phosphatase. Mol Endocrinol 25:474–481.

Kurisaki K, Kurisaki A, Valcourt U, Terentiev AA, Pardali K, Ten Dijke P, Heldin CH, Ericsson J, Moustakas A. 2003. Nuclear factor YY1 inhibits transforming growth factor beta- and bone morphogenetic protein-induced cell differentiation. Mol Cell Biol 23:4494–4510.

Komatsu M, Chiba T, Tatsumi K, Iemura S, Tanida I, Okazaki N, Ueno T, Kominami E, Natsume T, Tanaka K. 2004. A novel protein-conjugating system for Ufm1, a ubiquitin-fold modifier. EMBO J 23:1977–1986.

Lin X, Duan X, Liang YY, Su Y, Wrighton KH, Long J, Hu M, Davis CM, Wang J, Brunicardi FC, Shi Y, Chen YG, Meng A, Feng XH. 2006. PPM1A functions as a Smad phosphatase to terminate TGFbeta signaling. Cell 125:915–928.

Loughlin FE, Mansfield RE, Vaz PM, McGrath AP, Setiyaputra S, Gamsjaeger R, Chen ES, Morris BJ, Guss JM, Mackay JP. 2009. The zinc fingers of the SR-like protein ZRANB2 are single-stranded RNA-binding domains that recognize 5' splice site-like sequences. Proc Natl Acad Sci USA 106:5581–5586.

Mangs AH, Morris BJ. 2008. ZRANB2: Structural and functional insights into a novel splicing protein. Int J Biochem Cell Biol 40:2353–2357.

Miyazono K, Maeda S, Imamura T. 2005. BMP receptor signaling: Transcriptional targets, regulation of signals, and signaling cross-talk. Cytokine Growth Factor Rev 16:251–263.

Miyazono K, Maeda S, Imamura T. 2006. Smad Transcriptional Co-activators and Co-repressors. In: Ten Dijke P, Heldin CH, editors Smad signal transduction. Dordrecht Netherlands: Springer. pp 277–293.

Nakamura Y, Weidinger G, Liang JO, Aquilina-Beck A, Tamai K, Moon RT, Warman ML. 2007. The CCN family member Wisp3, mutant in progressive pseudorheumatoid dysplasia, modulates BMP and Wnt signaling. J Clin Invest 117:3075–3086.

Natsume T, Yamauchi Y, Nakayama H, Shinkawa T, Yanagida M, Takahashi N, Isobe T. 2002. A direct nanoflow liquid chromatography-tandem mass spectrometry system for interaction proteomics. Anal Chem 74:4725–4733.

Nojima J, Kanomata K, Takada Y, Fukuda T, Kokabu S, Ohte S, Takada T, Tsukui T, Yamamoto TS, Sasanuma H, Yoneyama K, Ueno N, Okazaki Y, Kamijo R, Yoda T, Katagiri T. 2010. Dual roles of smad proteins in the conversion from myoblasts to osteoblastic cells by bone morphogenetic proteins. J Biol Chem 285:15577–15586.

Ohte S, Shin M, Sasanuma H, Yoneyama K, Akita M, Ikebuchi K, Jimi E, Maruki Y, Matsuoka M, Namba A, Tomoda H, Okazaki Y, Ohtake A, Oda H, Owan I, Yoda T, Furuya H, Kamizono J, Kitoh H, Nakashima Y, Susami T, Haga N, Komori T, Katagiri T. 2011. A novel mutation of ALK2, L196P, found in the most benign case of fibrodysplasia ossificans progressiva activates BMP-specific intracellular signaling equivalent to a typical mutation, R206H. Biochem Biophys Res Commun 407:213–218.

Shen H, Green MR. 2006. RS domains contact splicing signals and promote splicing by a common mechanism in yeast through humans. Genes Dev 20:1755–1765.

Suzuki A, Thies RS, Yamaji N, Song JJ, Wozney JM, Murakami K, Ueno N. 1994. A truncated bone morphogenetic protein receptor affects dorsal-ventral patterning in the early Xenopus embryo. Proc Natl Acad Sci USA 91:10255–10259.

Suzuki T, Fujisawa JI, Toita M, Yoshida M. 1993. The trans-activator tax of human T-cell leukemia virus type 1 (HTLV-1) interacts with cAMP-responsive element (CRE) binding and CRE modulator proteins that bind to the 21-base-pair enhancer of HTLV-1. Proc Natl Acad Sci USA 90:610–614.

Urist MR. 1965. Bone: Formation by autoinduction. Science 150:893–899.

Wan M, Cao X. 2005. BMP signaling in skeletal development. Biochem Biophys Res Commun 328:651–657.

Wiemann S, Weil B, Wellenreuther R, Gassenhuber J, Glassl S, Ansorge W, Bocher M, Blocker H, Bauersachs S, Blum H, Lauber J, Dusterhoft A, Beyer A, Kohrer K, Strack N, Mewes HW, Ottenwalder B, Obermaier B, Tampe J, Heubner D, Wambutt R, Korn B, Klein M, Poustka A. 2001. Toward a catalog of human genes and proteins: Sequencing and analysis of 500 novel complete protein coding human cDNAs. Genome Res 11:422–435.

Wu JW, Krawitz AR, Chai J, Li W, Zhang F, Luo K, Shi Y. 2002. Structural mechanism of Smad4 recognition by the nuclear oncoprotein Ski: Insights on Ski-mediated repression of TGF-beta signaling. Cell 111:357–367.

Yu PB, Deng DY, Lai CS, Hong CC, Cuny GD, Bouxsein ML, Hong DW, McManus PM, Katagiri T, Sachidanandan C, Kamiya N, Fukuda T, Mishina Y, Peterson RT, Bloch KD. 2008a. BMP type I receptor inhibition reduces heterotopic ossification. Nat Med 14:1363–1369.

Yu PB, Hong CC, Sachidanandan C, Babitt JL, Deng DY, Hoyng SA, Lin HY, Bloch KD, Peterson RT. 2008b. Dorsomorphin inhibits BMP signals required for embryogenesis and iron metabolism. Nat Chem Biol 4:33–41.

Zhu H, Kavsak P, Abdollah S, Wrana JL, Thomsen GH. 1999. A SMAD ubiquitin ligase targets the BMP pathway and affects embryonic pattern formation. Nature 400:687–693.

MOLECULAR AND CELLULAR BIOLOGY, Nov. 2011, p. 4500–4512 Vol. 31, No. 22
0270-7306/11/$12.00 doi:10.1128/MCB.05663-11

Dual Regulation of the Transcriptional Activity of Nrf1 by β-TrCP- and Hrd1-Dependent Degradation Mechanisms▽

Yoshiki Tsuchiya,[1]† Tomoko Morita,[1]† Mehee Kim,[1] Shun-ichiro Iemura,[2] Tohru Natsume,[2] Masayuki Yamamoto,[3] and Akira Kobayashi[1]*

Laboratory for Genetic Cord, Graduate School of Life and Medical Sciences, Doshisha University, 1-3 Tatara Miyakodani, Kyotanabe 610-0394,[1] National Institutes of Advanced Industrial Science and Technology, Biological Information Research Center, Kohtoh-ku, Tokyo 135-0064,[2] and Department of Medical Biochemistry and ERATO-JST, Tohoku University Graduate School of Medicine, Aoba-ku, Sendai 980-8575,[3] Japan

Received 22 May 2011/Returned for modification 19 June 2011/Accepted 3 September 2011

A growing body of evidence suggests that Nrf1 is an inducible transcription factor that maintains cellular homeostasis. Under physiological conditions, Nrf1 is targeted to the endoplasmic reticulum (ER), implying that it translocates into the nucleus in response to an activating signal. However, the molecular mechanisms by which the function of Nrf1 is modulated remain poorly understood. Here, we report that two distinct degradation mechanisms regulate Nrf1 activity and the expression of its target genes. In the nucleus, β-TrCP, an adaptor for the SCF (Skp1-Cul1-F-box protein) ubiquitin ligase, promotes the degradation of Nrf1 by catalyzing its polyubiquitination. This activity requires a DSGLS motif on Nrf1, which is similar to the canonical β-TrCP recognition motif. The short interfering RNA (siRNA)-mediated silencing of β-TrCP markedly augments the expression of Nrf1 target genes, such as the proteasome subunit PSMC4, indicating that β-TrCP represses Nrf1 activation. Meanwhile, in the cytoplasm, Nrf1 is degraded and suppressed by the ER-associated degradation (ERAD) ubiquitin ligase Hrd1 and valosin-containing protein (VCP) under normal conditions. We identified a cytoplasmic degradation motif on Nrf1 between the NHB1 and NHB2 domains that exhibited species conservation. Thus, these results clearly suggest that both β-TrCP- and Hrd1-dependent degradation mechanisms regulate the transcriptional activity of Nrf1 to maintain cellular homeostasis.

The transcription factor Nrf1 (NF-E2-related factor 1 or NFE2L1) belongs to the cap'n'collar-type basic leucine zipper (CNC-bZip) protein family. Nrf1 activates gene expression through either the antioxidant response element (ARE) or the Maf recognition element (MARE) by heterodimerizing with small Maf proteins (14, 32). The physiological roles of Nrf1 remain unclear, but gene-targeting experiments have helped to elucidate the function of Nrf1. Nrf1-deficient mice display an embryonic lethal phenotype due to anemia (3). The conditional gene targeting of Nrf1 in hepatocytes, osteoblasts, and neural cells causes steatosis, diminished bone formation, and neurodegeneration, respectively (10, 13, 23, 36, 37). These *in vivo* observations clearly indicate that Nrf1 is indispensable to the maintenance of cellular homeostasis. Recent studies have demonstrated that Nrf1 regulates expression of a set of proteasome subunit genes to maintain proteasome homeostasis (27, 31). Extensive biochemical studies have also elucidated the molecular regulation of Nrf1. Under physiological conditions, Nrf1 is anchored to the endoplasmic reticulum (ER) by its N-terminal NHB1 domain (34, 40, 42). This finding suggests that Nrf1-mediated gene expression requires activating stresses or signals that lead to the liberation of Nrf1 from the ER and, thereby, the nuclear translocation of Nrf1. Supporting this idea, a number of studies have reported that several drugs, including tunicamycin, *tert*-butyl hydroquinone (tBHQ), ascorbic acid, and arsenite, promote the nuclear entry of Nrf1 (34, 36, 41, 44) although the precise mechanisms of their activities have not been fully elucidated.

The ubiquitin-proteasome system serves a central regulatory function by modulating the abundance of proteins in many biological processes, such as cell cycle progression, signal transduction, and transcription. The polyubiquitin chain, an important degradation signal recognized by the proteasome, is conjugated to substrate proteins by sequential reactions catalyzed by three types of enzymes (7, 28): the ubiquitin-activating enzymes (E1), the ubiquitin-conjugating enzymes (E2), and the ubiquitin ligases (E3). The E3 ubiquitin ligases exhibit two distinct functions; one function is to target substrate proteins, and the other function is to catalyze the formation of isopeptide bonds between the substrate protein and ubiquitin. Based on structural similarities, the E3 ubiquitin ligases are classified into three groups: the RING-finger proteins, the HECT domain proteins, and the U-box domain proteins. Among the RING-finger proteins, the SCF (Skp1-Cul1-F-box protein) ubiquitin ligases have been thoroughly characterized (5, 20). The SCF complex comprises the F-box protein, Skp1, and Cul1. The F-box protein functions as an adaptor that determines target specificity and recruits the target protein into the Cul1 scaffold along with Skp1. Sixty-nine F-box proteins, including β-TrCP (the β-transducin repeat-containing protein), have been identified in humans. β-TrCP regulates various cellular processes by mediating the degradation of target proteins,

* Corresponding author. Mailing address: Laboratory for Genetic Cord, Graduate School of Life and Medical Sciences, Doshisha University, 1-3, Tatara Miyakodani, Kyotanabe 610-0394, Japan. Phone: 81 774 65 6273. Fax: 81 774 65 6274. E-mail: akobayas@mail.doshisha.ac.jp.
† Y.T. and T.M. contributed equally to this paper.
▽ Published ahead of print on 12 September 2011.

such as IκB, β-catenin, and Cdc25, which are intimately related to tumorigenesis. Mammals express two distinct paralogues of this protein, β-TrCP1 and β-TrCP2, which exhibit similar biochemical properties (thus, the paralogues will here be referred to as β-TrCP). β-TrCP recognizes a consensus DpSGX$_n$pS motif ($n \geq 1$; pS represents the phosphorylated serine residue) or variants of this motif in its substrates via its WD40 repeat domain. In the case of the former canonical motif, phosphorylation of its conserved serine residues is indispensable for the recognition of specific substrates by β-TrCP. Numerous reports have documented that the phosphorylation of the substrates of β-TrCP is catalyzed by specific kinases, such as glycogen synthase kinase 3β (GSK-3β), polo-like kinase, and CK1.

The endoplasmic reticulum-associated degradation (ERAD) is a quality control system for misfolded or improperly assembled membrane proteins and secreted proteins in the ER (1, 8). Such aberrant proteins are polyubiquitinated by ubiquitin ligases, comprising multiple protein subunits, in the ER membrane. These components are conserved in all eukaryotic organisms, strongly suggesting the importance of this process to cellular homeostasis. One of the ERAD ubiquitin ligases, Hrd1 (also known as synoviolin), forms a complex with SEL1L and predominantly mediates the degradation of soluble, ER-luminal substrates and integral membrane proteins. After being polyubiquitinated by the Hrd1-SEL1L complex, the substrates are recognized by a complex containing the AAA-ATPase p97/valosin-containing protein (VCP) and are transported to the proteasome. Intriguingly, Hrd1 has been reported to control the turnover of p53 in the cytoplasm (38). This finding indicates that Hrd1 contributes to the degradation of cytoplasmic factors as well as ERAD.

To understand the physiological roles of Nrf1, we first attempted to elucidate the regulatory mechanism of Nrf1. In this regard, the growing body of evidence regarding the molecular basis of the stress response mediated by the Nrf1-related factor Nrf2 provided considerable insight. Nrf2 is one of the major regulatory factors to induce the expression of oxidative stress response genes, such as heme oxygenase-1 (*Ho-1*) and *Nqo1*, in response to oxidative stress (32). Under physiological conditions, Nrf2 is sequestered in the cytoplasm by the oxidative stress sensor Keap1. Moreover, Keap1 possesses an additional function as an adaptor protein for the Cul3-based ubiquitin ligase and, thereby, mediates the polyubiquitin conjugation and proteasomal degradation of Nrf2. Importantly, the nature of the activation mechanism of Nrf2 in response to oxidative stress is the inhibition of the Keap1-mediated ubiquitination of Nrf2, which results in the nuclear entry of stabilized Nrf2 (12). Based on these findings, we hypothesized that the function of Nrf1 is also regulated in a ubiquitin-proteasome-dependent fashion and investigated this hypothesis in the current study. Here, we report that the transcriptional activity of Nrf1 is modulated by two distinct degradation pathways in the nucleus and the cytoplasm. The nuclear degradation of Nrf1 is mediated by the ubiquitin ligase adaptor β-TrCP, which results in the repression of the transcriptional activity of Nrf1. The cytoplasmic degradation of Nrf1 is dependent on Hrd1 and VCP. Collectively, these results suggest that the regulation of two proteolysis pathways induces the transcriptional activation by Nrf1 to maintain cellular homeostasis.

MATERIALS AND METHODS

Antibodies. The antibodies utilized in this study included anti-Flag (M2; Sigma), anti-hemagglutinin ([HA] Y-11; Santa Cruz), anti-Myc (A-14; Santa Cruz), anti-green fluorescent protein ([GFP] B-2; Santa Cruz), anti-Nrf1 (H-285; Santa Cruz), anti-Nrf2 (H-300; Santa Cruz), anti-β-catenin (BD Biosciences), anti-α-tubulin (Sigma), and anti-lamin B1 (Zymed). The rat monoclonal anti-Keap1 antibody was described previously (35). Rat monoclonal antibodies directed against mouse Nrf1 were raised by immunizing rats with a purified recombinant Nrf1 protein (residues 211 to 460), tagged with six histidine residues, that was expressed in *Escherichia coli*. After hybridoma cells expressing antibodies were selected, one positive clone for Nrf1 (clone 17) was injected into the abdominal cavity of a mouse to produce ascites, and the resultant antibody was purified from ascites using a protein G column (Pierce).

Plasmid construction. All expression plasmids of Flag-tagged wild-type (WT) Nrf1 and deletion mutants were generated by subcloning the cDNA fragments encoding various Nrf1 mutants that were amplified by PCR into the Asp718 and XbaI sites of pcDNA3 (Invitrogen). HA-tagged wild-type β-TrCP2 and ΔF-box mutant expression vectors were kindly provided by Keiko Nakayama (Tohoku University). The HA–β-TrCP2 ΔWD40 expression vector was constructed through the PCR-based amplification method. The Myc-tagged β-TrCP2 expression vector was constructed by subcloning β-TrCP2 into the pcDNA3-Myc vector. The Flag-tagged Nrf2 was generated as described previously (9). The HA-tagged ubiquitin vector was kindly provided by Dirk Bohmann (33). The 3×PSMA4-ARE-Luc vector was kindly provided by Raymond J. Deshaies (27). All constructions were verified by DNA sequencing. Detailed information regarding all expression vectors is available upon request.

Cell culture and transfection. COS7 cells and HeLa cells were cultured in Dulbecco's modified Eagle's medium (DMEM) (Wako) supplemented with 10% fetal calf serum (FCS) (Invitrogen), 4,500 mg/liter glucose, 40 μg/ml streptomycin, and 40 units/ml penicillin. Mouse embryonic fibroblasts (MEFs) were cultured in Iscove's modified Dulbecco's medium (IMDM) (Wako) supplemented with 10% FCS, 2 mM glutamine (Invitrogen), 40 μg/ml streptomycin, and 40 units/ml penicillin. The transfection of plasmid DNA and short interfering RNA (siRNA) was achieved by Lipofectamine Plus and Lipofectamine 2000 (Invitrogen), respectively.

Immunoprecipitation and immunoblot analysis. Expression plasmids for wild-type or deletion mutants of HA–β-TrCP2 were transfected into COS7 cells along with wild-type or deletion mutants of Nrf1 with three copies of the Flag tag (3×Flag-Nrf1). At 24 h after transfection, cells were treated with the protease inhibitor MG132 (Peptide Institute) at a concentration of 10 μM for 8 h and subjected to preparation of whole-cell extracts with lysis buffer (50 mM Tris-HCl [pH 8.0], 10% glycerol, 100 mM NaF, 50 mM NaCl, 2 mM EDTA, 2 mM sodium orthovanadate, 10 mM sodium pyrophosphate, 10 mM β-glycerophosphate, 0.1% NP-40, and 1× protease inhibitor cocktail [Roche]). The whole-cell extracts were subjected to immunoprecipitation with anti-Flag M2 affinity gels (Sigma) at 4°C for 2 h. After the affinity gels were washed with a wash buffer (50 mM Tris-HCl [pH 7.4], 150 mM NaCl and 0.1% NP-40) three times, immunocomplexes were eluted by boiling in an SDS sample buffer (50 mM Tris-HCl [pH 6.8], 10% glycerol and 1% SDS) and subjected to immunoblot analysis using the antibodies indicated on the figures. The blots were treated with a horseradish peroxidase-conjugated secondary antibody (Invitrogen) and were developed with enhanced chemiluminescence (ECL; GE Healthcare).

Cycloheximide chase experiment. Expression vectors encoding wild-type 3×Flag-Nrf1 or deletion mutants were transfected into COS7 cells along with a GFP expression vector, which served as an internal control. At 24 h after transfection, the cells were treated with 20 μg/ml cycloheximide, and at the indicated time points, the whole-cell extracts were prepared and subjected to immunoblot analysis with the antibodies indicated on the figures. For the analysis of endogenous proteins, the cells were pretreated with 10 μM MG132 for 6 h, washed two times with phosphate-buffered saline (PBS), and treated with 20 μg/ml cycloheximide.

Subcellular fractionation of MEFs. MEFs derived from wild-type and Nrf1 knockout mice were grown in six-well plates and left untreated or treated with 10 μM MG132 for 8 h. The method of the preparation of cytoplasmic and nuclear extracts was described previously (12). Briefly, the cells were swollen in buffer A (20 mM HEPES-KOH [pH 8.0], 10 mM KCl, 1.5 mM $MgCl_2$, 0.1 mM EDTA, 1 mM dithiothreitol [DTT], 1× protease inhibitor cocktail [Roche], and 10 μM MG132), followed by lysis with the addition of NP-40 (at a final concentration of 2.5%). After centrifugation, the supernatants and precipitates were collected. The supernatants were further subjected to centrifugation at 20,000 × *g* for 10 min, and subsequent supernatants were employed as cytoplasmic extracts in the present study. On the other hand, the precipitates were subjected to two washes

with buffer A, lysis with the SDS sample buffer, and mild sonication to shear genomic DNA. After centrifugation, the supernatants were collected as nuclear extracts. The quantities of proteins in these extracts were determined with a bicinchoninic acid (BCA) kit (Thermo).

Immunocytochemical staining. COS7 cells transiently expressing wild-type 3×Flag-tagged Nrf1 or a deletion mutant or HA–β-TrCP2 were fixed with formaldehyde for 10 min, washed twice with PBS, and permeabilized with 0.5% Triton X-100 in PBS for 5 min. The cells were washed with PBS twice and treated with anti-Flag or anti-HA antibodies for 1 h at room temperature. After cells were washed three times with PBS, they were incubated with Alexa 488- or Alexa 546-conjugated secondary antibodies for 30 min at room temperature, and the nuclei were stained with 4′,6′-diamidino-2-phenylindole (DAPI). After samples were washed with PBS, a drop of fluorescent mounting medium (Dako) was placed on the glass slides. Fluorescence images were captured by an Olympus IX71 microscope.

siRNA knockdown experiment. HeLa cells split into 12-well plates were cultured for 24 h in medium without antibiotics. The cells were transfected twice with 40 nM siRNA (at 24 and 48 h after plating) using Lipofectamine 2000 (Invitrogen). At 24 h after the last transfection, the cells were utilized for each experiment. For the cotransfection of siRNA and plasmid DNA, 40 nM siRNA was transfected into the cells along with plasmid DNA using Lipofectamine 2000 (Invitrogen). A GFP expression vector was also transfected into the cells as an internal control. At 24 h after transfection, the culture medium was replaced with fresh medium without antibiotics, and the cells were subsequently cultured for 24 h. The cells were lysed with an SDS sample buffer, and the resultant whole-cell extracts were subjected to immunoblot analysis with the antibodies indicated on the figures. The sequences of the sense strand of the siRNA duplexes employed in the present study were as follows: control siRNA, 5′-UUCUCCGAACGUGUCACGUdTdT-3′; Nrf1, 5′-GGGA UUCGGUGAAGAUUUGdTdT-3′; β-TrCP1(1), 5′-CAAAUCUUCACCGAA UCCCdTdT-3′; β-TrCP1(2), 5′-UUCUCACAGGCCAUACAGGdTdT-3′; β-TrCP2, 5′-GAGGCCAUCAGAAGGAAACdTdT-3′; β-TrCP1/2, 5′-GUGG AAUUUGUGGAACAUCdTdT-3′; Keap1, 5′-GGCCUUUGGCAUCAUGA ACdTdT-3′; VCP, 5′-GUAGGGUAUGAUGACAUUGdTdT-3′; gp78, 5′-CA UGCAGAAUGUCUCUUAAdTdT-3′; TEB4, 5′-UUAAGAGUGUGCUGCC UAAdTdT-3′. For the knockdown of Hrd1, siGENOME SMART pools of four oligonucleotide duplexes targeted against Hrd1 (Dharmacon) were used.

RNA extraction and real-time quantitative PCR. Total RNA was extracted from cells with an RNeasy Mini kit (Qiagen) and subjected to cDNA synthesis with random hexamer primers. Real-time quantitative PCR was performed with FastStart Universal SYBR (Roche) master mix and an ABI Prism 7900 (Applied Biosystems). The PCR primers employed in the present study were as follows: Nrf1, 5′-TGGAACAGCAGTGGCAAGATCTCA-3′ and 5′-GGCACTGTACA GGATTTCACTTGC-3′; β-TrCP1, 5′-TGCCGAAGTGAAACAAGC-3′ and 5′-CCTGTGAGAATTCGCTTG-3′; β-TrCP2, 5′-TCAGTGGCCTACGAGAT A-3′ and 5′-ACACGCTCATCATACTGCA-3′; glyceraldehyde-3-phosphate dehydrogenase (GAPDH), 5′-CCAGAACATCATCCCTGCCTCTACT-3′ and 5′-GGTTTTTCTAGACGGCAGGTCAG-3′; 18S rRNA, 5′-CGCCGCTAGAGG TGAAATTC-3′ and 5′-CGAACCTCCGACTTTCGTTCT-3′; Psmc4, 5′-GGA AGACCATGTTGGCAAAG-3′ and 5′-AAGATGATGGCAGGTGCATT-3′; Psma2, 5′-GCCCCGATTACAGAGTGC-3′ and 5′-TGGACGAACACCACCT GA-3′; Psma4, 5′-CATTGGCTGGGATAAGCA-3′ and 5′-ATGCATGTGGC CTTCCAT-3′; VCP, 5′-TACCAACCGGCCTGACAT-3′ and 5′-TGGCAACA CGGGACTTCT-3′; Hrd1, 5′-TGCAACCACATTTTCCATACCA-3′ and 5′-G CGATGCACGAAGGACATC-3′; gp78, 5′-GGTGCAGCGTAAGGACGA A-3′ and 5′-GCATCATCTTCAGAACTTTTGTTCA-3′; TEB4, 5′-TTGTCCT TCCAAGTCCGCCAG-3′ and 5′-GACTGTGGAGGTGGTGGAGATG-3′.

The ubiquitination assay. HeLa cells were transfected with expression plasmids encoding 3×Flag-Nrf1 P3 (Nrf1 with a deletion of residues 1 to 242) and HA-tagged ubiquitin along with plasmids expressing wild-type Myc-tagged β-TrCP2 or a ΔF-box β-TrCP2 mutant. At 24 h after transfection, the cells were treated with 10 μM MG132 for 8 h and were lysed with lysis buffer (10 mM Tris-HCl [pH 7.5], 150 mM NaCl, 1% SDS, 1× protease inhibitor cocktail [Roche], 10 μM MG132, and 10 mM *N*-ethylmaleimide [NEM]) to prepare the whole-cell extracts. The cell extracts were immediately boiled and diluted with dilution buffer (10 mM Tris-HCl [pH 7.5], 150 mM NaCl, 1% Triton X-100, 1× protease inhibitor cocktail, 10 μM MG132, and 10 mM NEM). After centrifugation at 18,000 × *g* for 15 min, the supernatants were incubated with anti-Flag antibody and protein G Sepharose beads (GE Healthcare) at 4°C for 2 h. The immunocomplexes were washed with dilution buffer twice and were eluted by boiling in an SDS sample buffer. Ubiquitinated Nrf1 was visualized by immunoblot analysis using anti-HA antibody.

Luciferase assay. The day before transfection, COS7 cells were split into 24-well plates and cultured for 24 h. The cells were transfected with plasmids encoding 3×Flag-Nrf1 P3 or the P3-SA mutant (with alanine substitutions at two serine residues of the motif Ser448/451) along with luciferase reporter plasmids encoding the NQO1 promoter (9) or three tandem copies of the ARE of PSMA4 (27), and cells were transfected with pRL-TK (Promega) as an internal control. At 24 h after transfection, luciferase activities were measured with the PicaGene luciferase assay system (Toyo Ink) and a Berthold Lumat LB9507 luminometer.

Statistical analysis. Data comparisons were conducted with a two-tailed Student's *t* test for repeated measurements.

RESULTS

The transcription factor Nrf1 is degraded in both the cytoplasm and the nucleus. To evaluate our hypothesis that the biological function of Nrf1 is regulated in a proteasome-dependent manner, we first examined whether the proteasome inhibitor MG132 stabilizes the endogenous Nrf1 protein. We treated wild-type MEFs with MG132 for 8 h and prepared cytoplasmic and nuclear extracts from the cells. The expression level of Nrf1 was determined by immunoblot analysis with anti-Nrf1 antibody. The result indicates that MG132 treatment significantly enhanced multiple immunoreactive bands at 110 kDa (Fig. 1A, lanes 1 to 4). In contrast, MG132 treatment of Nrf1 knockout mouse-derived MEFs did not cause an increase in the immunoreactive bands (Fig. 1A, lanes 5 to 8), suggesting that the immunoreactive bands were derived from the endogenous Nrf1. Thus, we conclude that the turnover of Nrf1 is strongly dependent on proteasome activity.

This result also demonstrates that the Nrf1 protein accumulated predominantly in the nucleus upon treatment with MG132. As it has been reported that Nrf1 is localized to the ER membrane under normal conditions, we assumed that Nrf1 is constitutively degraded in the cytoplasm and that, after MG132 treatment, Nrf1 is stabilized and translocates into the nucleus. To test this hypothesis, we attempted to identify the cellular compartment where Nrf1 degradation occurs. Overexpressed wild-type (WT) full-length Nrf1 was localized to both the cytoplasm and the nucleus (Fig. 1B and C, WT). Thus, we generated Nrf1 mutants that predominantly localized to either the cytoplasm or the nucleus. As prior studies have reported that Nrf1 possesses an ER retention motif in the NHB1 domain and a nuclear localization signal (NLS) in the basic region of the bZip domain, we constructed Nrf1 mutants that lacked the NHB1 domain (P1) or the bZip domain (ΔbZip) (Fig. 1B). The subcellular localization of these Nrf1 mutants expressed in COS7 cells was determined by immunocytochemical staining with anti-Flag antibody. The result clearly indicates that the P1 mutant and the ΔbZip mutant predominantly localized to the nucleus and the cytoplasm, respectively (Fig. 1C). Utilizing these Nrf1 mutants, we investigated whether these mutant proteins undergo proteasome-mediated degradation. MG132 treatment stabilized wild-type Nrf1, implying that this assay closely mimics the degradation mechanism of endogenous Nrf1. Interestingly, not only the ΔbZip mutant but also the P1 mutant were significantly stabilized by MG132 treatment (Fig. 1D). This result clearly indicates that both mutant proteins are effectively degraded in a proteasome-dependent manner and strongly suggests that Nrf1 is degraded in both the cytoplasm and the nucleus.

β-TrCP mediates the nuclear degradation of Nrf1. To decipher the molecular basis underlying the cytoplasmic and nu-

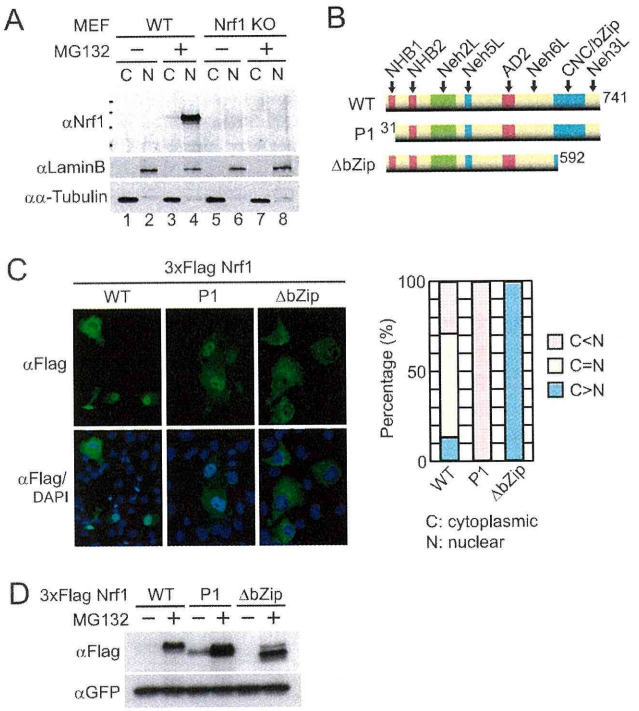

FIG. 1. The proteasomal degradation of the transcription factor Nrf1 in the cytoplasm and the nucleus. (A) MG132 stabilized the endogenous Nrf1 in MEFs. MEFs derived from wild-type (WT) and Nrf1 knockout (Nrf1 KO) mice were treated with MG132 (10 μM) for 8 h. Cytoplasmic (C) and nuclear (N) extracts from the cells were subjected to immunoblot analysis with rat monoclonal anti-Nrf1 antibody. Lamin B1 and α-tubulin were utilized as nuclear and cytoplasmic markers, respectively. (B) Schematic structures of the wild type and of the P1 and ΔbZip deletion mutants of Nrf1. The domain nomenclature was defined previously (40). The numbers denote the positions of the amino acid residues in the complete sequence of Nrf1. (C) The P1 and ΔbZip Nrf1 mutants predominantly localized in the nucleus and the cytoplasm, respectively, of COS7 cells. Nrf1 wild-type and mutants were stained with anti-Flag antibody, and the nuclei were stained with DAPI. A bar graph depicts the results of a quantitative analysis of the subcellular localization of the Nrf1 wild-type and mutants. More than 100 transfected cells were observed for the expression of each plasmid and classified into three different categories: C < N, nucleus-dominant staining; C = N, roughly equal distribution between the cytoplasmic and nuclear compartments; C > N, cytoplasm-dominant staining. (D) Both the P1 and ΔbZip Nrf1 mutants were degraded by the proteasome in COS7 cells. Cells were treated with MG132 (10 μM) for 8 h, and the expression levels of Nrf1 wild-type and deletion mutants were analyzed by immunoblot analysis with anti-Flag antibody. GFP was coexpressed as an internal control. α, anti.

clear degradation of Nrf1, we attempted to identify the molecular component(s) that regulates Nrf1 proteolysis by using a proteomic approach (21). Whole-cell extracts from HEK293 cells expressing C-terminal Flag-tagged Nrf1 were subjected to immunoprecipitation with anti-Flag antibody to isolate Nrf1 complexes. Subsequent liquid chromatography-tandem mass spectrometry (LC-MS/MS) analyses identified a variety of proteins, including transcriptional cofactors, kinases, and protein modification enzymes, as Nrf1-associated molecules (data not shown). Importantly, the ubiquitination-related factors β-TrCP2, Skp1, and Keap1 were identified as Nrf1-binding factors. The β-TrCP2-Skp1 heterodimer and Keap1 are substrate-specific adaptors for the Cul1- and Cul3-based ubiquitin ligase complexes, respectively. Accordingly, we performed siRNA-mediated RNA interference experiments to examine whether β-TrCP2 and Keap1 are involved in the mechanism of Nrf1 degradation. Taking into consideration the functional redundancy between β-TrCP2 and its analogue β-TrCP1, we first examined the effect of siRNA against β-TrCP1, β-TrCP2, or both proteins (β-TrCP1/2) on the stability of Flag-tagged Nrf1 expressed in HeLa cells. Whole-cell extracts were prepared from the cells and were subjected to immunoblot analysis with anti-Flag antibody to examine the expression level of Nrf1. As a result, the knockdown of both β-TrCP1 and β-TrCP2 significantly stabilized the Nrf1 protein, whereas the knockdown of β-TrCP2 alone demonstrated a much smaller effect on Nrf1 stability (Fig. 2A). The silencing efficiency of β-TrCP1 and β-TrCP2 was confirmed by a real-time quantitative PCR analysis (Fig. 2B). Therefore, we employed siRNA specific to both β-TrCP1 and β-TrCP2 in all subsequent experiments. Next, we investigated the effect of β-TrCP siRNA on the stability of the Nrf1 mutants. Interestingly, β-TrCP siRNA significantly stabilized the P1 mutant but not the ΔbZip mutant while MG132 treatment stabilized both mutants (Fig. 2C). Real-time quantitative PCR analysis demonstrated that the β-TrCP siRNA significantly reduced both β-TrCP1 and β-TrCP2 mRNAs but not Nrf1 mRNA (Fig. 2D). These data indicate that Nrf1 degradation is regulated by both β-TrCP-dependent and -independent mechanisms. Given that the P1 and ΔbZip mutants exhibit distinct intracellular localizations (Fig. 1C), it is likely that β-TrCP-dependent degradation of Nrf1 occurs predominantly in the nucleus. Meanwhile, Keap1 siRNA did not stabilize the wild-type Nrf1 or the P1 or ΔbZip mutant (Fig. 2C and E, left panel) although it stabilized Nrf2 (Fig. 2E, right panel). These results indicate that Keap1 is not involved in the regulation of Nrf1 degradation.

To confirm further the β-TrCP-dependent degradation of Nrf1, we addressed the question of whether β-TrCP siRNA stabilizes the endogenous Nrf1 protein. Unexpectedly, β-TrCP siRNA alone did not stabilize Nrf1 in HeLa cells (data not shown), probably because the endogenous Nrf1 is predominantly localized to the ER membrane and is primarily degraded in the cytoplasm rather than in the nucleus. Because MG132 treatment causes the nuclear accumulation of Nrf1 in MEFs (Fig. 1A), we performed cycloheximide chase experiments using HeLa cells pretreated with MG132. As a result, β-TrCP siRNA significantly suppressed the degradation of the endogenous Nrf1 (Fig. 2F, 1/2) as well as that of β-catenin, a canonical β-TrCP substrate. Taken together, these findings indicate that β-TrCP regulates the nuclear degradation of Nrf1.

Colocalization and physical interaction of Nrf1 and β-TrCP. To understand the molecular basis of the β-TrCP-mediated degradation of Nrf1, we investigated the subcellular colocalization of Nrf1 and β-TrCP2 by immunostaining. The 3×Flag-tagged Nrf1 and HA-tagged β-TrCP2 expressed in COS7 cells were visualized with anti-Flag and anti-HA antibodies, respectively. We observed significant colocalization of Nrf1 and β-TrCP2 (Fig. 3A). Next, we assessed the physical interaction between Nrf1 and β-TrCP2 by immunoprecipitation analysis. Whole-cell extracts from COS7 cells expressing both factors were subjected to immunoprecipitation with anti-Flag anti-

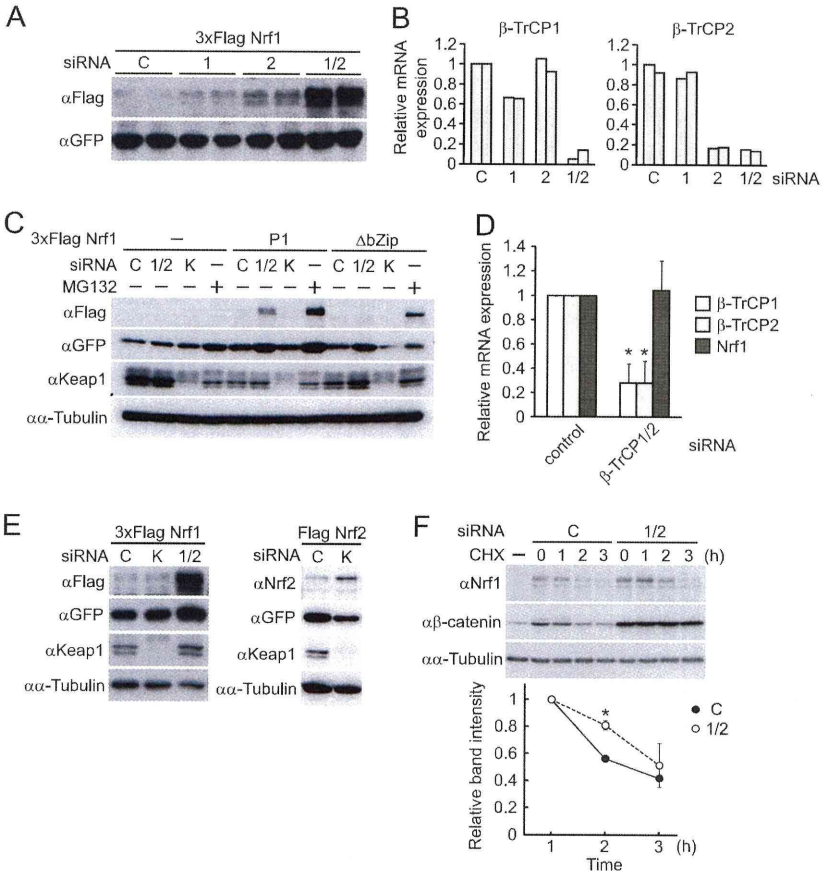

FIG. 2. The β-TrCP protein regulates the nuclear degradation of Nrf1. (A) HeLa cells were transfected with the 3×Flag-Nrf1 and GFP expression vectors at 24 h after two rounds of transfection with control (C), β-TrCP1 (1), β-TrCP2 (2), or β-TrCP1/2 (1/2) siRNA. At 24 h after the last transfection, whole-cell extracts were prepared and subjected to immunoblot analysis. Duplicate samples are presented. (B) The knockdown efficiency of each siRNA for β-TrCP1 and β-TrCP2 was determined by real-time quantitative PCR analysis. Duplicate samples are presented. (C) HeLa cells were transfected with siRNA against β-TrCP1 and β-TrCP2 (1/2), Keap1 (K), or the control (C) along with 3×Flag-tagged P1 and the ΔbZip Nrf1 mutant. Cells were left untreated or treated with MG132 (10 μM) for 8 h. Cell extracts were subjected to immunoblot analysis with the indicated antibodies. (D) Real-time quantitative PCR analysis revealed that siRNA directed against β-TrCP significantly reduced mRNA expression of both β-TrCP1 and β-TrCP2 but not Nrf1 in HeLa cells. The values were normalized with GAPDH and are presented as the means ± standard deviations ($n = 3$; *, $P < 0.001$). (E) Control (C), Keap1 (K), or β-TrCP1/2 (1/2) siRNA was transfected into HeLa cells in combination with the 3×Flag-Nrf1 vector or the Flag Nrf2 vector. Whole-cell extracts were subjected to immunoblot analysis with the indicated antibodies. (F) The siRNA directed against β-TrCP stabilized the endogenous Nrf1. β-TrCP (1/2) or the control (C) siRNA was twice transfected into HeLa cells. At 48 h after the second transfection, the cells were pretreated with MG132 (10 μM) for 6 h and treated with cycloheximide (CHX) (20 μg/ml). Whole-cell extracts were prepared for immunoblot analysis with anti-Nrf1 (H-285) antibody. The β-catenin protein is a canonical β-TrCP substrate, and α-tubulin is an internal control. The graph depicts the quantified band intensities of Nrf1. The values were normalized with α-tubulin and are presented as the means ± standard error ($n = 3$; *, $P < 0.005$). The values at 1 h after cycloheximide treatment were set to 1.

body-conjugated beads. Immunoblot analysis with anti-HA antibody revealed that β-TrCP2 was coimmunoprecipitated with Nrf1 (Fig. 3B). These results demonstrate that β-TrCP interacts with Nrf1.

Identification of the association interfaces between Nrf1 and β-TrCP. We then defined the association interfaces between Nrf1 and β-TrCP with an immunoprecipitation assay. To this end, we generated a series of deletion mutants of β-TrCP2 and Nrf1 (Fig. 3C and E). The β-TrCP protein is composed of the F-box and WD40 repeat domains, and the latter is known as the substrate-binding domain. An immunoprecipitation assay demonstrated that deletion of the WD40 repeat domain, but not the F-box domain, from β-TrCP2 significantly compromised its interaction with Nrf1 (Fig. 3D, ΔWD), indicating that β-TrCP2 interacts with Nrf1 via the WD40 repeat domain.

Next, we analyzed the β-TrCP binding region within Nrf1. We coexpressed a series of 3×Flag-tagged, N-terminal deletion mutants of Nrf1 with HA-tagged β-TrCP2 in COS7 cells. Nrf1 mutants were then immunoprecipitated with anti-Flag antibody, and the precipitates were analyzed by immunoblotting. The result clearly indicates that the P2 (Nrf1 with a deletion of residues 1 through 106) and P3 mutants associate with β-TrCP but that the P4 mutant (deletion of residues 1 through 463) did not (Fig. 3F, lanes 3 to 7), indicating that residues 243 to 463 of Nrf1 could be recognized by β-TrCP. On the other hand, the analysis using internal deletion mutants of

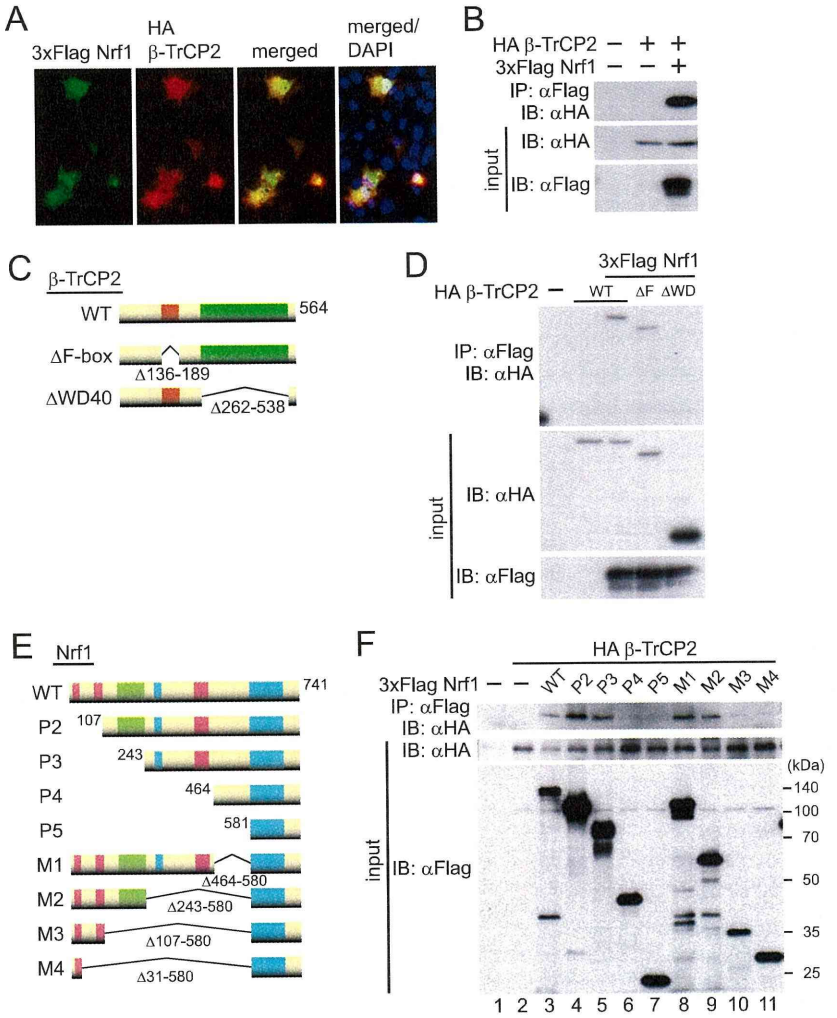

FIG. 3. Colocalization and physical interaction of Nrf1 with β-TrCP2. (A) Colocalization of wild-type Nrf1 with β-TrCP2 in COS7 cells. The 3×Flag-Nrf1 and HA–β-TrCP2 expressed in COS7 cells were immunostained with the indicated antibodies. (B) Physical interaction of Nrf1 with β-TrCP2. Whole-cell extracts of COS7 cells expressing 3×Flag-Nrf1 and HA-tagged β-TrCP2 were subjected to immunoprecipitation (IP) with anti-Flag antibody, followed by immunoblot (IB) analysis with the indicated antibodies. (C) Schematic structures of β-TrCP2 deletion mutants. β-TrCP2 comprises the F-box and WD40 repeat domains. (D) The WD40 repeat domain of β-TrCP2 was required for its association with Nrf1. The 3×Flag-Nrf1 and the HA–β-TrCP2 wild type (WT) or ΔF-box (ΔF) or ΔWD40 (ΔWD) mutant were expressed into COS7 cells, and immunoprecipitation with anti-Flag antibody was performed, as described above. (E) Schematic structures of Nrf1 deletion mutants. (F) Identification of β-TrCP2-binding regions within Nrf1. Immunoprecipitation with anti-Flag antibody was performed, as described above. To ensure that the Nrf1 mutant proteins were expressed at similar levels, we transfected various amounts of plasmids, as follows: WT and M1, 1 μg; P2, P3, and M2, 0.3 μg; P4, P5, M3, and M4, 30 ng.

Nrf1 indicates that the M2 mutant, but not the M3 mutant, can interact with β-TrCP. Thus, residues 107 to 242 may represent another β-TrCP-binding interface (Fig. 3F, lanes 8 to 11). These results collectively indicate that at least two regions within Nrf1 can interact with β-TrCP.

An internal region (residues 243 to 463) of Nrf1 is required for its β-TrCP-dependent nuclear degradation. To further identify the amino acid region responsible for the β-TrCP-dependent degradation of Nrf1, we examined the effect of β-TrCP knockdown on the stability of Nrf1 mutants. In N-terminal deletion analysis, β-TrCP siRNA stabilized the P2 and P3 Nrf1 mutants, as well as wild-type Nrf1 (Fig. 4A, lanes 3 to 8). However, β-TrCP siRNA did not change the expression level of the P4 mutant (Fig. 4A, lanes 9 and 10). This result implies that the internal region (residues 243 to 463) but not residues 107 to 242 is required for the β-TrCP-dependent degradation of Nrf1. Consistent with this result, internal deletion analysis revealed that β-TrCP siRNA stabilized the M1 mutant (Nrf1 with a deletion of residues 464 through 580) but not the M2 mutant (Nrf1 with a deletion of residues 243 through 580) (Fig. 4A, lanes 11 to 14), emphasizing the functional significance of the region (residues 243 to 463) in the regulation of Nrf1 proteolysis. This result also indicates that the region (residues 107 to 242) is not able to mediate β-TrCP-dependent degradation. Accordingly, we conclude that β-TrCP regulates Nrf1 stability through its internal region (residues 243 to 463).

We also examined the stability of deletion mutants of Nrf1

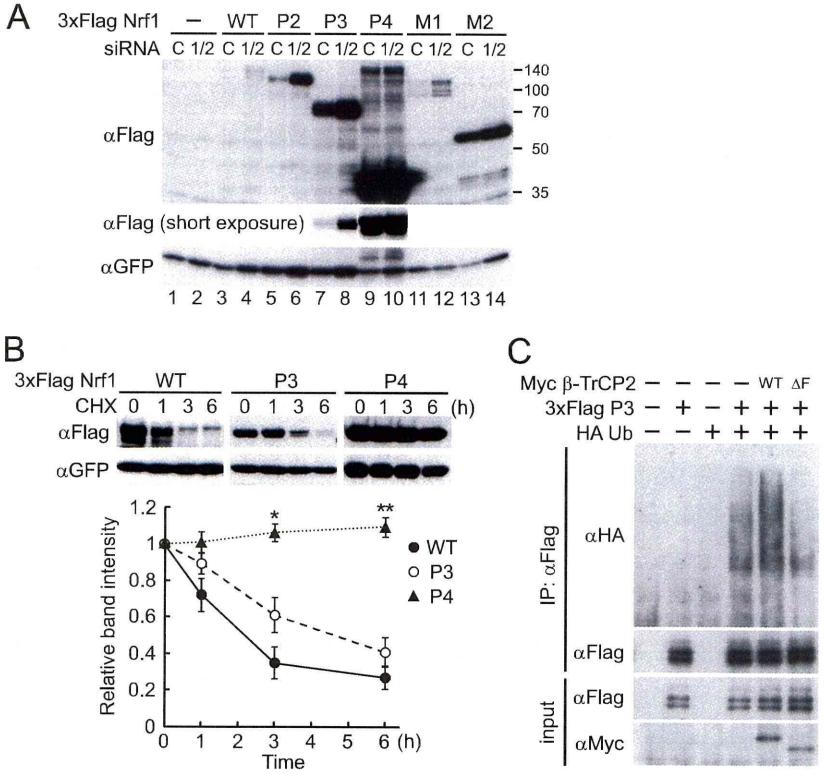

FIG. 4. A region (residues 243 to 463) of Nrf1 is required for its β-TrCP-mediated degradation. (A) The Nrf1 mutants lacking amino acid residues 243 to 463 were not stabilized by the siRNA-mediated knockdown of β-TrCP. Control (C) or β-TrCP (1/2) siRNA was transfected into HeLa cells in combination with the indicated Nrf1 mutants. The expression levels of the mutants were analyzed, as described in the legend to Fig. 2C. (B) The deletion of residues 243 to 463 significantly stabilized Nrf1. HeLa cells were transfected with the expression plasmid for the wild type or the P3 or P4 mutant of 3×Flag-Nrf1. Next, the cells were treated with cycloheximide (CHX) (20 μg/ml), and the whole-cell extracts were prepared at the indicated time points. The assays were performed three times. Data normalized with cotransfected GFP are presented as the means ± standard errors ($n = 3$; *, $P < 0.005$; **, $P < 0.001$ versus wild type). (C) The β-TrCP-dependent polyubiquitination of Nrf1 in cultured cells. HeLa cells were transfected with the P3 Nrf1 mutant, HA-ubiquitin (Ub), and the Myc β-TrCP2 wild type (WT) or ΔF-box (ΔF) mutant. The P3 mutant was immunoprecipitated (IP) by anti-Flag antibody, and its ubiquitination was detected by immunoblot analysis with anti-HA antibody.

by cycloheximide chase experiments to determine whether the internal region identified above is essential for the proteolytic degradation of Nrf1. As a result, the N-terminal-deleted P3 Nrf1 mutant continued to undergo efficient degradation although it was slightly stabilized compared with wild-type Nrf1 (Fig. 4B). In contrast, the P4 mutant, which lacks amino acid residues 243 to 463, was significantly stabilized, indicating that the regulatory motif that is required for the nuclear degradation of Nrf1 resides in this internal region. Overall, we conclude that β-TrCP regulates the nuclear degradation of Nrf1 by associating with its internal region (residues 243 to 463).

β-TrCP mediates the polyubiquitination of Nrf1. To examine whether β-TrCP mediates the ubiquitination of Nrf1, we performed a ubiquitination assay in cultured cells. The 3×Flag-tagged P3 Nrf1 mutant and Myc-tagged β-TrCP2 were cotransfected into HeLa cells along with HA-tagged ubiquitin. The whole-cell extracts were subjected to immunoprecipitation with anti-Flag antibody-conjugated beads, and ubiquitination of the P3 mutant was detected by immunoblotting with anti-HA antibody. This result demonstrates that the ubiquitination of the P3 mutant is markedly enhanced by the coexpression of wild-type β-TrCP2 (Fig. 4C, WT). In addition, the coexpression of the ΔF-box mutant of β-TrCP2 resulted in reduced ubiquitination of the P3 mutant (Fig. 4C, ΔF). Thus, we conclude that β-TrCP catalyzes the polyubiquitination of Nrf1 and leads to its proteasome-mediated degradation.

Identification of the β-TrCP-recognition motif (DSGLS) within Nrf1. β-TrCP has been characterized as recognizing the consensus motif DpSGX$_n$pS ($n \geq 1$; pS represents the phosphorylated serine residue) present in its substrates. We found that certain amino acid sequences (residues 243 to 463) of Nrf1 contain a similar motif, namely, DSGLS (Fig. 5A). Importantly, this motif is highly conserved among species and in other NF-E2-related factors including p45/NF-E2, Nrf2, and Nrf3. Indeed, like Nrf1, Nrf2 was stabilized by knockdown of β-TrCP (Fig. 5B). Prior studies have indicated that the erythropoietin receptor (EpoR) and the YAP transcription coactivator also contain a DSGXS motif that functions as a β-TrCP recognition motif (Fig. 5A) (17, 43). To examine whether this motif is required for the β-TrCP-mediated degradation of Nrf1, we introduced alanine substitutions at two serine residues of the motif Ser448/451, which appear to be the critical phosphorylation sites for β-TrCP binding. We examined the stability of the resultant P3-SA mutant with cycloheximide

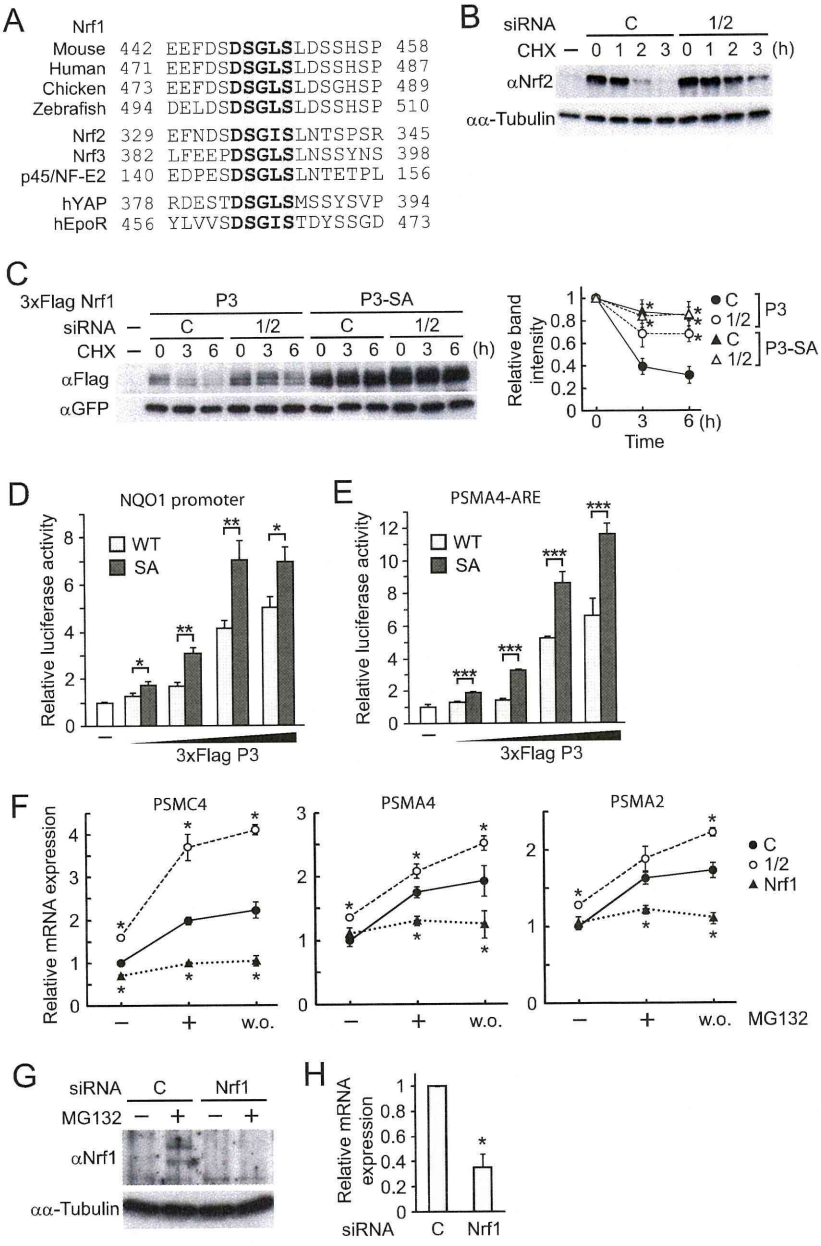

FIG. 5. A DSGLS motif is required for the β-TrCP-mediated degradation of Nrf1. (A) Alignment of Nrf1 sequences among species and NF-E2-related factors around the highly conserved DSGLS motif, which is similar to the β-TrCP recognition motifs of the human YAP and erythropoietin receptor (EpoR). Shaded areas denote conserved serine residues that were replaced with alanine for subsequent experiments. (B) β-TrCP siRNA stabilized endogenous Nrf2. Transfection of siRNA and subsequent cycloheximide chase were performed, as described in the legend to Fig. 2F. (C) Alanine substitution of serine residues in the DSGLS motif (P3-SA) stabilized the P3 Nrf1 mutant. At 48 h after transfection of siRNA and Nrf1 mutant constructs, the cycloheximide chase experiment was conducted, as described in the legend to Fig. 4B. Assays were performed three times. The values were normalized with GFP and presented as the means ± standard errors ($n = 3$; *, $P < 0.05$ versus P3 with control siRNA). (D and E) A nuclear degradation mechanism repressed the transcriptional activity of Nrf1. COS7 cells were transfected with either P3 (WT) or P3-SA (SA) Nrf1 mutant plasmid in combination with a luciferase reporter containing a single ARE of NQO1 gene (D) or three tandem copies of ARE of PSMA4 (E). The levels of luciferase activity were normalized with the *Renilla* luciferase activity of an internal control pRL-TK, and results are presented as the means ± standard deviations ($n = 3$ [D] and $n = 4$ [E]; *, $P < 0.05$; **, $P < 0.01$; ***, $P < 0.001$). (F) β-TrCP is involved in the regulation of the expression of Nrf1 target genes induced by proteasome inhibition. HeLa cells transfected twice with the indicated siRNA were left untreated (−) or were treated with (+) MG132 (1 μM) for 16 h, and then MG132-treated cells were incubated without MG132 for another 3 h (w.o.). The mRNA expression levels were determined by real-time quantitative PCR analysis. The values were normalized with 18S rRNA and are presented as the means ± standard deviations ($n = 3$; *, $P < 0.05$ versus control siRNA). (G and H) The siRNA-mediated knockdown of Nrf1. HeLa cells were twice transfected with control (C) or Nrf1 siRNA. At 24 h after the second transfection, Nrf1 knockdown efficiency was determined by immunoblot analysis with anti-Nrf1 (H-285) antibody (G) or by real-time quantitative PCR analysis (H). For immunoblot analysis, cells were treated with MG132 (10 μM) for 8 h. The values were normalized with 18S rRNA and are presented as the means ± standard deviations ($n = 4$; *, $P < 0.001$).

chase experiments. While the degradation of the P3 mutant was efficiently suppressed by siRNA-mediated β-TrCP knockdown, as expected, the P3-SA mutant was significantly stabilized even in the absence of β-TrCP siRNA (Fig. 5C). Thus, these data clearly indicate that the DSGLS motif is required for the β-TrCP-mediated degradation of Nrf1.

β-TrCP-mediated degradation represses the transcriptional activity of Nrf1. The involvement of β-TrCP in the regulation of Nrf1 stability prompted us to investigate the effect of the knockdown of β-TrCP on the transcriptional activity of Nrf1. The ubiquitin-proteasome pathway has been reported to activate transcription by regulating a variety of transcriptional factors (15, 19). Our hypothesis was that a nuclear degradation mechanism is required to achieve Nrf1-mediated transcription after its activation. To test our hypothesis, we compared the transcriptional activity of the P3 and P3-SA mutants in a luciferase reporter assay using COS7 cells. We first utilized a luciferase reporter driven by the NQO1 promoter, which contained the Nrf1 recognition sequence ARE (9). Forced expression of the P3 mutant increased reporter activity in a dose-dependent manner (Fig. 5D), indicating that this mutant retains transcriptional activity. Notably, the P3-SA mutant exhibited enhanced transcriptional activity compared with that of the P3 mutant (Fig. 5D). This result suggests that β-TrCP-mediated degradation of Nrf1 is involved in the repression of Nrf1-dependent transcription. Recent reports have indicated that Nrf1 regulates the expression of a set of proteasome subunit genes in response to the proteasome inhibition (27, 31). We then utilized another luciferase reporter that contains three copies of the ARE of the PSMA4 promoter (27). The result was similar to that obtained with the NQO1 promoter (Fig. 5E). To further clarify the role of β-TrCP in Nrf1-mediated transcription, we examined the effect of β-TrCP knockdown on the expression of endogenous proteasome subunit genes induced by proteasome inhibition. The expression of PSMC4, PSMA4, and PSMA2 was induced by the treatment of HeLa cells with MG132 for 16 h, and this induction was significantly repressed by the siRNA knockdown of Nrf1 (Fig. 5F, Nrf1 and C). Efficient silencing of Nrf1 was confirmed at both the protein and the mRNA levels (Fig. 5G and H). This result indicates that the induction of these genes is highly dependent on Nrf1. Under this situation, the siRNA knockdown of β-TrCP significantly enhanced the expression of PSMC4, PSMA4, and PSMA2 induced by MG132 (Fig. 5F, 1/2 and C). This enhancement persisted after the washing out of MG132. These results clearly demonstrate that β-TrCP is involved in the repression of the transcriptional activation of Nrf1 target genes such as the proteasome subunit genes.

Hrd1 and VCP mediate the cytoplasmic degradation of Nrf1. We investigated the molecular mechanism underlying the cytoplasmic degradation of Nrf1. In keeping with a recent report demonstrating that Nrf1 is degraded via the ERAD pathway (31), the siRNA knockdown of VCP, an AAA-ATPase required for protein transport from the ER to the proteasome during ERAD, increased the quantity of the endogenous Nrf1 protein in HeLa cells (Fig. 6A). In addition, among several ERAD-related E3 ligases, the knockdown of Hrd1 specifically increased the expression of the Nrf1 protein. The efficient silencing of these genes was confirmed by a real-time quantitative PCR analysis (Fig. 6B). A cycloheximide chase experiment further revealed that the knockdown of VCP or Hrd1 significantly stabilized the Nrf1 protein (Fig. 6C). Notably, the electrophoretic mobility of Nrf1 was altered by the knockdown of VCP or Hrd1, suggesting that the limited proteolysis and/or posttranslational modification of Nrf1 was impaired (see Discussion). The knockdown of other ERAD E3 ligases, gp78 and TEB4, did not stabilize Nrf1 (Fig. 6C). These results indicate that Nrf1 undergoes cytoplasmic degradation via the Hrd1-dependent ERAD pathway.

We next investigated whether transcriptional activity of Nrf1 is suppressed by cytoplasmic degradation via the ERAD pathway. We examined the effect of siRNA knockdown of Hrd1 on the expression of Nrf1 target genes. The result shows that siRNA against Hrd1 as well as β-TrCP significantly enhanced proteasome subunit gene expression, suggesting that cytoplasmic degradation functions to suppress Nrf1 activity (Fig. 6D).

An amino acid region (residues 31 to 81) is required for the cytoplasmic degradation of Nrf1. Finally, we attempted to identify an amino acid region responsible for the cytoplasmic degradation of Nrf1. As demonstrated in Fig. 2, the ΔbZip Nrf1 mutant that localized in the cytoplasm was degraded in a β-TrCP-independent manner. Accordingly, we first generated two ΔbZip mutants, one lacking the N-terminal region (ΔbZip-1) and the other lacking the Neh2L domain, which shares considerable homology with the Keap1-interacting domain in Nrf2 (ΔbZip-2) (Fig. 6E). Immunocytochemical staining confirmed the predominant cytoplasmic localization of the mutants (data not shown). The stability of these mutant proteins was determined by a cycloheximide chase experiment. As a result, significant stabilization of the ΔbZip mutant was observed when its N-terminal region was deleted (Fig. 6F, ΔbZip-1), implying that this region is required for the cytoplasmic degradation of Nrf1. In contrast, the deletion of the Neh2L domain did not affect the stability of the ΔbZip mutant (Fig. 6F, ΔbZip-2), reemphasizing that Keap1 is not involved in the cytoplasmic degradation of Nrf1. We further introduced a series of deletions in the N-terminal region of the ΔbZip mutant and analyzed the stability of these mutants (Fig. 6E, ΔbZip-3 to ΔbZip-6). Deletion of either the NHB1 domain or the NHB2 domain did not alter the stability of the ΔbZip mutant protein (Fig. 6G, ΔbZip-3 and ΔbZip-5). In contrast, the deletion of a short region (residues 31 to 81) located between the NHB1 and NHB2 domains markedly stabilized the ΔbZip mutant protein (Fig. 6G, ΔbZip-4 and ΔbZip-6). These results indicate that the region in question (residues 31 to 81) is required for the cytoplasmic degradation of Nrf1. The genome database indicates that this region is highly conserved among species and is partially conserved in Nrf3, thereby suggesting its functional significance in the degradation of Nrf1 (Fig. 6H). Taken together, our data indicate that the cytoplasmic degradation of Nrf1 is regulated by a small region between the NHB1 and NHB2 domains, which is not associated with the β-TrCP-mediated degradation of Nrf1.

DISCUSSION

In this study, we investigated the mechanisms by which the transcriptional activity of Nrf1 is modulated to sustain cellular homeostasis. We determined that β-TrCP- and Hrd1-dependent degradation mechanisms regulate the biological activity

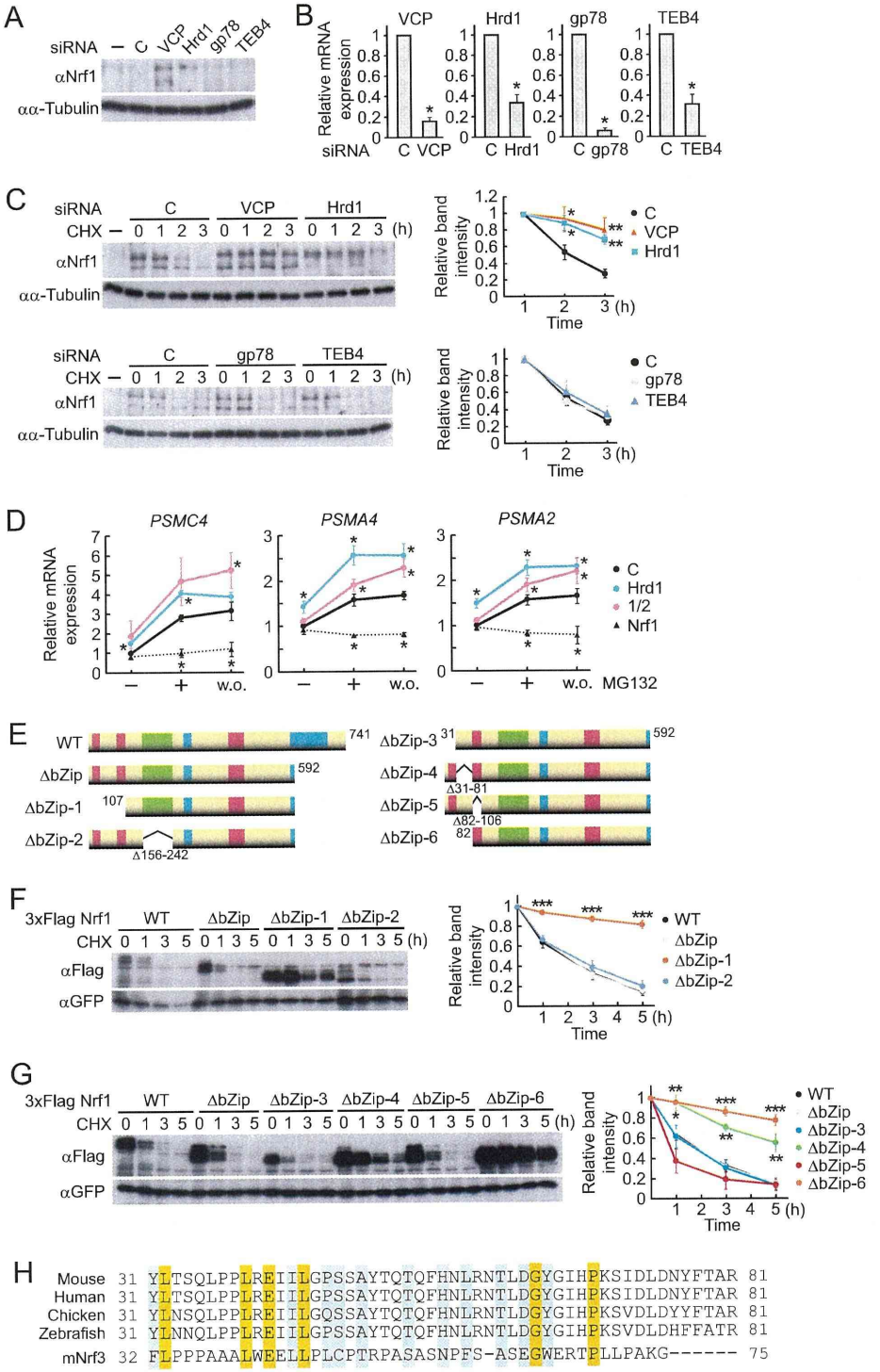

FIG. 6. Hrd1 and VCP regulate the cytoplasmic degradation of Nrf1. (A) VCP or Hrd1 siRNA stabilized endogenous Nrf1 in HeLa cells. Transfection was carried out twice. The whole-cell extracts were prepared and analyzed by immunoblotting with anti-Nrf1 (H-285) antibody. α-Tubulin is an internal control. (B) Knockdown efficiency of ERAD-related E3 ligases. A knockdown experiment was conducted as described in the legend to Fig. 5H. The values were normalized with 18S rRNA and are presented as the means ± standard deviations ($n = 4$; *, $P < 0.001$). (C) Knockdown of VCP and Hrd1 inhibited Nrf1 degradation. Transfection of siRNA and subsequent cycloheximide chase were performed, as described in the legend to Fig. 2F. Data are presented as the means ± standard errors ($n = 5$; *, $P < 0.05$; **, $P < 0.01$ versus control siRNA). (D) Hrd1 is involved in the regulation of the expression of Nrf1 target genes induced by proteasome inhibition. The assays were performed according to the legend of Fig. 5F. Data are presented as the means ± standard deviations ($n = 3$; *, $P < 0.05$ versus control siRNA). (E) Schematic structures of deletion mutants derived from the ΔbZip Nrf1 mutant. (F and G) A region (residues 31 to 81) of Nrf1 is required for the cytoplasmic degradation of Nrf1. Cycloheximide chase experiments using the Nrf1 deletion mutants were performed according to the legend of Fig. 4B. Data are presented as the means ± standard errors ($n = 7$ [F]; $n \geq 3$ [G]; *, $P < 0.05$; **, $P < 0.005$; ***, $P < 0.001$ versus wild-type Nrf1). (H) Amino acid residues (31 to 81) of mouse Nrf1 are highly conserved among species and in mouse Nrf3 (mNrf3). Shaded amino acid positions highlight amino acid identity (orange) or similarity (blue) between Nrf1 and Nrf3.

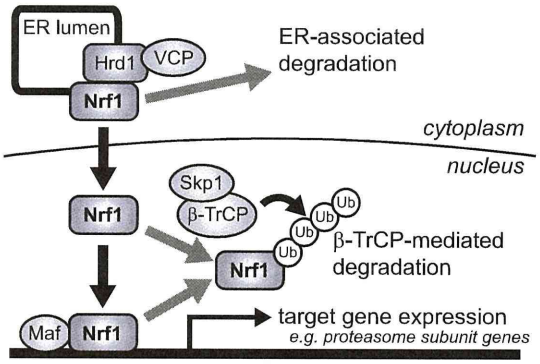

FIG. 7. A model for the dual mechanisms of Nrf1 degradation in regulating the expression of Nrf1 target genes. Nrf1 is degraded via the ERAD pathway under physiological conditions. Upon activation, Nrf1 is stabilized and translocates into the nucleus. In the nucleus, β-TrCP-mediated degradation prevents inappropriate transcription of Nrf1 target genes such as proteasome subunit genes. This degradation may also facilitate the clearance of Nrf1 from the nucleus after the activation of Nrf1 is abolished. Ub, ubiquitin.

of Nrf1 in the nucleus and the cytoplasm, respectively. Under homeostatic conditions, Nrf1 is sequestered in the ER through its NHB1 domain and undergoes proteasomal degradation in an Hrd1-dependent manner. Upon exposure to activating signals, Nrf1 evades degradation and activates expression of its target genes. After Nrf1 produces biological responses, its activity is terminated by the β-TrCP-dependent degradation process. Also, this study is the first to demonstrate that β-TrCP is involved in the regulation of proteasome subunit gene expression. Our schematic model in Fig. 7 summarizes the regulatory mechanism of Nrf1, which is tightly coupled with two distinct degradation pathways.

Multiple lines of evidence suggest that a cytoprotection system is a double-edged sword; specifically, constitutive activation of the system rather alters homeostatic balances (16). For example, our group and other investigators have identified that the aberrant activation of the oxidative stress response by somatic mutations to the *NRF2* and *KEAP1* genes provides growth advantages and anticancer drug resistance to human lung cancer cells (22, 24, 29, 30). These findings strongly suggest that the precise repression of the stress response system under nonstressed conditions is also indispensable for cellular homeostasis. In this regard, two discrete proteolysis pathways contribute to the suppression of the inappropriate activation of Nrf1. The cytoplasmic degradation mechanism achieves the complete repression of Nrf1 activity, as well as its retention in the ER. Moreover, the nuclear degradation pathway also prevents unnecessary expression of Nrf1 target genes under physiological conditions and may resolve the gene activation after stress termination. Given that Nrf1 upregulates expression of proteasome subunit genes in response to proteasome inhibition, two distinct degradation mechanisms should strictly regulate Nrf1 activity to maintain proteasome homeostasis.

We identified the DSGLS motif in Nrf1. This motif resembles the canonical β-TrCP recognition sequence (DpSGX$_n$pS), and similar sequences are found in EpoR and the transcriptional coactivator YAP (17, 43). The DSGX$_n$S motif usually requires phosphorylation to associate with β-TrCP. In fact, alanine substitutions at the conserved serine residues (Ser448 and Ser451) in the Nrf1 P3 mutant markedly compromised the β-TrCP-dependent degradation of Nrf1 (Fig. 5C). This finding suggests the involvement of the phosphorylation of the DSGLS motif in the β-TrCP-dependent degradation of Nrf1. We found that lithium chloride (LiCl), a potent but nonselective GSK-3 inhibitor, slightly stabilized Nrf1; however, SB216763, a more selective inhibitor of GSK-3, did not (data not shown). Thus, further analyses are required to identify the kinase(s) responsible for the phosphorylation of the DSGLS motif and the regulatory mechanism of the nuclear degradation of Nrf1. Because the DSGLS motif is highly conserved in NF-E2-related factors (p45/NF-E2, Nrf1, Nrf2, and Nrf3), the β-TrCP-mediated degradation mechanism might be a common regulatory pathway among these transcription factors. In accordance with our result, a study published during the preparation of the manuscript demonstrated that Nrf2 possesses the DSGLS motif and is degraded by β-TrCP in a Keap1-independent manner (26). Thus, unlike Keap1, β-TrCP might be a common factor in the repression of the gene expression induced by NF-E2-related factors.

We do not exclude the possibility that β-TrCP is positively involved in transcriptional activation by Nrf1. As shown in Fig. 5C to E, the transcriptional activity of the P3-SA mutant was not strongly increased, in spite of its significant stabilization. This finding may indicate that β-TrCP-mediated proteolysis contributes to both the resolution and the activation of transcriptional processes by Nrf1. Multiple lines of evidence suggest that the ubiquitin-proteasome pathway can activate transcription by regulating a variety of transcriptional factors (15, 19). For instance, the F-box protein Fbw7a promotes degradation of the steroid receptor coactivator SRC-3, consequently increasing the turnover of SRC-3 on the promoters of target genes and activating their transcription. Alternatively, the cooperative interaction of β-TrCP with the transcriptional coactivator p300/CBP enhances the expression of β-catenin-regulated genes (11). Because CBP activates the transcriptional activity of Nrf1 via the Neh5L domain (39), β-TrCP may synergistically recruit p300/CBP on Nrf1 and promote transcriptional activation by Nrf1 as well as its proteolysis.

A remaining important issue regarding the biological function of Nrf1 is the mechanism by which Nrf1 is liberated from ER sequestration and then activates gene expression. In this regard, we consider two possibilities. First, the inhibition of Hrd1-mediated degradation in the cytoplasm may lead to the nuclear translocation of Nrf1. We observed that MG132 treatment promotes the nuclear accumulation of the endogenous Nrf1 in MEFs and HeLa cells (Fig. 1A and data not shown). In addition, Nrf1 has been reported to mediate the induction of proteasome subunit genes after proteasome inhibition in mammalian cells (27, 31). These results imply that the suppression of cytoplasmic degradation allows Nrf1 to translocate into the nucleus and activate gene expression. In this hypothetical model, Nrf1 would function to recover proteasome activity by upregulating expression of proteasome subunit genes under a situation of proteasome dysfunction. Our current study determined that the cytoplasmic stability of Nrf1 is modulated by the ERAD-related ubiquitin ligase Hrd1 and VCP (Fig. 6A and C). Although the regulatory mechanisms of the Hrd1- and VCP-mediated proteasomal degradation pathways remain ob-

scure, further analysis might demonstrate that the inhibition of cytoplasmic degradation is the mechanism of Nrf1 activation.

A second possibility is that proteolytic cleavage may release Nrf1 from ER sequestration. For example, the ER-embedded transcription factors ATF-6 and SREBP (sterol regulatory element binding protein) translocate to the Golgi compartment in response to activating signals and are sequentially cleaved by Site-1 and Site-2 proteases, thereby resulting in their nuclear entry and their activation of target genes (2, 18). Indeed, we found that nuclearly accumulated Nrf1 migrated slightly more quickly than its cytoplasmically localized form in the gels (Fig. 1A). In addition, silencing of VCP and Hrd1 altered the electrophoretic mobility of Nrf1 (Fig. 6C). These results suggest that the cleavage of Nrf1 is also essential for its liberation from the ER. In this model, Hrd1 may eliminate the ER-accumulated Nrf1 that is not cleaved by a protease under nonstress conditions. To examine our two current hypotheses, further proteomics-based or genetic experiments to identify Nrf1-associated molecules may shed light on this issue.

Discussing the Nrf1 degradation mechanism from the perspective of molecular evolution would be interesting. The transcription factors *Caenorhabditis elegans* Skn-1 and *Drosophila* CncC are considered to be ancestral genes of NF-E2-related factors and activate the expression of oxidative stress response genes (32). Intriguingly, both factors are also regulated by proteasomal degradation (4, 6, 25). For instance, Skn-1 is degraded through polyubiquitination by the WDR-23/Cul4/DDB1 ubiquitin ligase under physiological conditions (4). Exhibiting similarity to the structure of β-TrCP, WDR-23 contains a WD40 repeat domain and functions as a ubiquitin ligase adaptor. The degradation process of Skn-1 is mediated by the p38 mitogen-activated protein (MAP) kinase, GSK-3, and the insulin-like receptor pathways, suggesting the presence of phosphorylation-dependent regulation. CncC is controlled by both Keap1-dependent and -independent proteasomal pathways (6). Notably, CncC also regulates the gene expression of proteasome subunits. Because Skn-1 and CncC do not possess the DSGLS motif, β-TrCP may not be involved in the regulation of these factors. Nevertheless, these transcription factors share the characteristic that their transcriptional activities are regulated by the ubiquitin-proteasome system. We surmise that the NF-E2-related factors underwent molecular evolution from these ancestral genes by acquiring the DSGLS motif and subsequently switching to the β-TrCP-mediated regulatory system. Such an evolutionary process may have conferred biological diversity and complexity to these transcription factors.

ACKNOWLEDGMENTS

We are grateful to Keiko Nakayama, Raymond J. Deshaies, and Dirk Bohmann for the β-TrCP2 plasmids, 3×PSMA4-ARE-Luc, and HA ubiquitin, respectively. We also thank Tomoki Chiba, Takako Tsukide, Akiko Matsumoto, and Jun Takai for research support.

This work was supported in part by grants-in-aid from the Ministry of Education, Sports, Science and Technology (A.K., Y.T., and M.Y.), the Mochida Memorial Foundation (A.K.), the Naito Foundation (A.K.), the Suzuken Memorial Foundation (A.K.), the Takeda Science Foundation (A.K.), the Inamori Foundation (Y.T.), and the Uehara Memorial Foundation (Y.T.).

REFERENCES

1. **Bagola, K., M. Mehnert, E. Jarosch, and T. Sommer.** 2011. Protein dislocation from the ER. Biochim. Biophys. Acta **1808:**925–936.
2. **Brown, M. S., J. Ye, R. B. Rawson, and J. L. Goldstein.** 2000. Regulated intramembrane proteolysis: a control mechanism conserved from bacteria to humans. Cell **100:**391–398.
3. **Chan, J. Y., et al.** 1998. Targeted disruption of the ubiquitous CNC-bZIP transcription factor, Nrf-1, results in anemia and embryonic lethality in mice. EMBO J. **17:**1779–1787.
4. **Choe, K. P., A. J. Przybysz, and K. Strange.** 2009. The WD40 repeat protein WDR-23 functions with the CUL4/DDB1 ubiquitin ligase to regulate nuclear abundance and activity of SKN-1 in *Caenorhabditis elegans*. Mol. Cell. Biol. **29:**2704–2715.
5. **Frescas, D., and M. Pagano.** 2008. Deregulated proteolysis by the F-box proteins SKP2 and β-TrCP: tipping the scales of cancer. Nat. Rev. Cancer **8:**438–449.
6. **Grimberg, K. B., A. Beskow, D. Lundin, M. M. Davis, and P. Young.** 2011. Basic-leucine zipper protein Cnc-C is a substrate and transcriptional regulator of the *Drosophila* 26S proteasome. Mol. Cell. Biol. **31:**897–909.
7. **Hershko, A.** 2005. The ubiquitin system for protein degradation and some of its roles in the control of the cell-division cycle (Nobel lecture). Angew. Chem. Int. Ed. Engl. **44:**5932–5943.
8. **Hosokawa, N., Y. Kamiya, and K. Kato.** 2010. The role of MRH domain-containing lectins in ERAD. Glycobiology **20:**651–660.
9. **Kang, M. I., A. Kobayashi, N. Wakabayashi, S. G. Kim, and M. Yamamoto.** 2004. Scaffolding of Keap1 to the actin cytoskeleton controls the function of Nrf2 as key regulator of cytoprotective phase 2 genes. Proc. Natl. Acad. Sci. U. S. A. **101:**2046–2051.
10. **Kim, J., W. Xing, J. Wergedal, J. Y. Chan, and S. Mohan.** 2010. Targeted disruption of nuclear factor erythroid-derived 2-like 1 in osteoblasts reduces bone size and bone formation in mice. Physiol. Genomics **40:**100–110.
11. **Kimbrel, E. A., and A. L. Kung.** 2009. The F-box protein β-TrCp1/Fbw1a interacts with p300 to enhance β-catenin transcriptional activity. J. Biol. Chem. **284:**13033–13044.
12. **Kobayashi, A., et al.** 2006. Oxidative and electrophilic stresses activate Nrf2 through inhibition of ubiquitination activity of Keap1. Mol. Cell. Biol. **26:**221–229.
13. **Kobayashi, A., et al.** 2011. Central nervous system-specific deletion of transcription factor Nrf1 causes progressive motor neuronal dysfunction. Genes Cells **16:**692–703.
14. **Kobayashi, M., and M. Yamamoto.** 2006. Nrf2-Keap1 regulation of cellular defense mechanisms against electrophiles and reactive oxygen species. Adv. Enzyme Regul. **46:**113–140.
15. **Lonard, D. M., and B. W. O'Malley.** 2008. SRC-3 transcription-coupled activation, degradation, and the ubiquitin clock: is there enough coactivator to go around in cells? Sci. Signal. **1:**pe16.
16. **Luo, J., N. L. Solimini, and S. J. Elledge.** 2009. Principles of cancer therapy: oncogene and non-oncogene addiction. Cell **136:**823–837.
17. **Meyer, L., et al.** 2007. β-Trcp mediates ubiquitination and degradation of the erythropoietin receptor and controls cell proliferation. Blood **109:**5215–5222.
18. **Mori, K.** 2003. Frame switch splicing and regulated intramembrane proteolysis: key words to understand the unfolded protein response. Traffic **4:**519–528.
19. **Muratani, M., and W. P. Tansey.** 2003. How the ubiquitin-proteasome system controls transcription. Nat. Rev. Mol. Cell Biol. **4:**192–201.
20. **Nakayama, K. I., and K. Nakayama.** 2006. Ubiquitin ligases: cell-cycle control and cancer. Nat. Rev. Cancer **6:**369–381.
21. **Natsume, T., et al.** 2002. A direct nanoflow liquid chromatography-tandem mass spectrometry system for interaction proteomics. Anal. Chem. **74:**4725–4733.
22. **Ohta, T., et al.** 2008. Loss of Keap1 function activates Nrf2 and provides advantages for lung cancer cell growth. Cancer Res. **68:**1303–1309.
23. **Ohtsuji, M., et al.** 2008. Nrf1 and Nrf2 play distinct roles in activation of antioxidant response element-dependent genes. J. Biol. Chem. **283:**33554–33562.
24. **Padmanabhan, B., et al.** 2006. Structural basis for defects of Keap1 activity provoked by its point mutations in lung cancer. Mol. Cell **21:**689–700.
25. **Page, B. D., S. J. Diede, J. R. Tenlen, and E. L. Ferguson.** 2007. EEL-1, a Hect E3 ubiquitin ligase, controls asymmetry and persistence of the SKN-1 transcription factor in the early *C. elegans* embryo. Development **134:**2303–2314.
26. **Rada, P., et al.** 2011. SCF/β-TrCP promotes glycogen synthase kinase 3-dependent degradation of the Nrf2 transcription factor in a Keap1-independent manner. Mol. Cell. Biol. **31:**1121–1133.
27. **Radhakrishnan, S. K., et al.** 2010. Transcription factor Nrf1 mediates the proteasome recovery pathway after proteasome inhibition in mammalian cells. Mol. Cell **38:**17–28.
28. **Ravid, T., and M. Hochstrasser.** 2008. Diversity of degradation signals in the ubiquitin-proteasome system. Nat. Rev. Mol. Cell Biol. **9:**679–690.
29. **Shibata, T., et al.** 2008. Cancer related mutations in *NRF2* impair its recog-

nition by Keap1-Cul3 E3 ligase and promote malignancy. Proc. Natl. Acad. Sci. U. S. A. **105:**13568–13573.
30. **Singh, A., et al.** 2006. Dysfunctional KEAP1-NRF2 interaction in non-small-cell lung cancer. PLoS Med. **3:**e420.
31. **Steffen, J., M. Seeger, A. Koch, and E. Kruger.** 2010. Proteasomal degradation is transcriptionally controlled by TCF11 via an ERAD-dependent feedback loop. Mol. Cell **40:**147–158.
32. **Sykiotis, G. P., and D. Bohmann.** 2010. Stress-activated cap'n'collar transcription factors in aging and human disease. Sci. Signal. **3:**re3.
33. **Treier, M., L. M. Staszewski, and D. Bohmann.** 1994. Ubiquitin-dependent c-Jun degradation in vivo is mediated by the delta domain. Cell **78:**787–798.
34. **Wang, W., and J. Y. Chan.** 2006. Nrf1 is targeted to the endoplasmic reticulum membrane by an N-terminal transmembrane domain. Inhibition of nuclear translocation and transacting function. J. Biol. Chem. **281:**19676–19687.
35. **Watai, Y., et al.** 2007. Subcellular localization and cytoplasmic complex status of endogenous Keap1. Genes Cells **12:**1163–1178.
36. **Xing, W., et al.** 2007. Nuclear factor-E2-related factor-1 mediates ascorbic acid induction of osterix expression via interaction with antioxidant-responsive element in bone cells. J. Biol. Chem. **282:**22052–22061.
37. **Xu, Z., et al.** 2005. Liver-specific inactivation of the Nrf1 gene in adult mouse leads to nonalcoholic steatohepatitis and hepatic neoplasia. Proc. Natl. Acad. Sci. U. S. A. **102:**4120–4125.
38. **Yamasaki, S., et al.** 2007. Cytoplasmic destruction of p53 by the endoplasmic reticulum-resident ubiquitin ligase "Synoviolin." EMBO J. **26:**113–122.
39. **Zhang, J., et al.** 2007. Nrf2 Neh5 domain is differentially utilized in the transactivation of cytoprotective genes. Biochem. J. **404:**459–466.
40. **Zhang, Y., D. H. Crouch, M. Yamamoto, and J. D. Hayes.** 2006. Negative regulation of the Nrf1 transcription factor by its N-terminal domain is independent of Keap1: Nrf1, but not Nrf2, is targeted to the endoplasmic reticulum. Biochem. J. **399:**373–385.
41. **Zhang, Y., J. M. Lucocq, and J. D. Hayes.** 2009. The Nrf1 CNC/bZIP protein is a nuclear envelope-bound transcription factor that is activated by t-butyl hydroquinone but not by endoplasmic reticulum stressors. Biochem. J. **418:**293–310.
42. **Zhang, Y., J. M. Lucocq, M. Yamamoto, and J. D. Hayes.** 2007. The NHB1 (N-terminal homology box 1) sequence in transcription factor Nrf1 is required to anchor it to the endoplasmic reticulum and also to enable its asparagine-glycosylation. Biochem. J. **408:**161–172.
43. **Zhao, B., L. Li, K. Tumaneng, C. Y. Wang, and K. L. Guan.** 2010. A coordinated phosphorylation by Lats and CK1 regulates YAP stability through $SCF^{\beta\text{-}TRCP}$. Genes Dev. **24:**72–85.
44. **Zhao, R., et al.** 2011. Long isoforms of NRF1 contribute to arsenic-induced antioxidant response in human keratinocytes. Environ. Health Perspect. **119:**56–62.

Intracellular phosphatidylserine is essential for retrograde membrane traffic through endosomes

Yasunori Uchida[a,1], Junya Hasegawa[a,1], Daniel Chinnapen[b], Takao Inoue[a], Seiji Okazaki[c], Ryuichi Kato[c], Soichi Wakatsuki[c], Ryo Misaki[d], Masato Koike[e], Yasuo Uchiyama[e], Shun-ichiro Iemura[f], Tohru Natsume[f], Ryusuke Kuwahara[g], Takatoshi Nakagawa[h], Kiyotaka Nishikawa[i], Kojiro Mukai[a], Eiji Miyoshi[j], Naoyuki Taniguchi[k], David Sheff[l], Wayne I. Lencer[b], Tomohiko Taguchi[a,2], and Hiroyuki Arai[a,2]

[a]Department of Health Chemistry, Graduate School of Pharmaceutical Sciences, University of Tokyo, Tokyo 113-0033, Japan; [b]Department of Gastrointestinal Cell Biology, Children's Hospital and Department of Pediatrics, Harvard Medical School, Boston, MA 02115; [c]Structural Biology Research Center, Photon Factory, Institute of Materials Structure Science, High Energy Accelerator Research Organization (KEK), Tsukuba, Ibaraki 305-0801, Japan; [d]International Center for Biotechnology, Osaka University, 2-1 Yamadaoka, Suita, Osaka 565-0871, Japan; [e]Department of Cell Biology and Neuroscience, Juntendo University School of Medicine, Tokyo 113-8421, Japan; [f]Biomedicinal Information Research Center, National Institute of Advanced Industrial Science and Technology, 2-4-7 Aomi, Koto-ku, Tokyo 135-0064, Japan; [g]Department of Biochemistry, Osaka University Graduate School of Medicine, Osaka 565-0871, Japan; [h]Department of Pharmacology, Osaka Medical College, Takatsuki, Osaka 569-8686, Japan; [i]Faculty of Life and Medical Sciences, Doshisha University, Kyoto 610-0394, Japan; [j]Department of Molecular Biochemistry and Clinical Investigation, Division of Health Science, Osaka University Graduate School of Medicine, Osaka 565-0871, Japan; [k]Systems Glycobiology Research Group, Advanced Science Institute, RIKEN, Wako, Saitama 351-0198, Japan; and [l]Department of Pharmacology, Carver College of Medicine, University of Iowa, Iowa City, IA 52242

Edited* by Kai Simons, Max Planck Institute of Molecular Cell Biology and Genetics, Dresden, Germany, and approved August 10, 2011 (received for review June 6, 2011)

Phosphatidylserine (PS) is a relatively minor constituent of biological membranes. Despite its low abundance, PS in the plasma membrane (PM) plays key roles in various phenomena such as the coagulation cascade, clearance of apoptotic cells, and recruitment of signaling molecules. PS also localizes in endocytic organelles, but how this relates to its cellular functions remains unknown. Here we report that PS is essential for retrograde membrane traffic at recycling endosomes (REs). PS was most concentrated in REs among intracellular organelles, and evectin-2 (evt-2), a protein of previously unknown function, was targeted to REs by the binding of its pleckstrin homology (PH) domain to PS. X-ray analysis supported the specificity of the binding of PS to the PH domain. Depletion of evt-2 or masking of intracellular PS suppressed membrane traffic from REs to the Golgi. These findings uncover the molecular basis that controls the RE-to-Golgi transport and identify a unique PH domain that specifically recognizes PS but not polyphosphoinositides.

cholera toxin | endocytosis

Phosphatidylserine (PS) is an anionic phospholipid class in eukaryotic biomembranes. PS is highly enriched in the plasma membrane (PM) and plays key roles in various physiological processes such as the coagulation cascade, recruitment and activation of signaling molecules, and clearance of apoptotic cells (1). These functions of PS are known to be executed by a number of proteins that have PS-recognition modules, such as a gamma-carboxyglutamic acid domain in prothrombin (2), a C2 domain in protein kinase C (3), a discoidin-type C2 domain in lactadherin (4), and a kinase associated-1 domain in MARK/PAR1 kinases (5). PS is also found in endocytic organelles (4, 6), where its functions are largely unknown.

Proteins newly synthesized at the endoplasmic reticulum (ER) that are destined for secretion or for residence within organelles move through the Golgi to their final destinations (7). This membrane outflow is counteracted by retrograde membrane flow that originates from either the PM or the endosomal system (8). The retrograde membrane traffic to the Golgi is used by several Golgi proteins to maintain their predominant Golgi localization, such as mannose 6-phosphate receptors (acid-hydrolase receptors), furin (a transmembrane enzyme), TGN38/46 (*trans*-Golgi resident proteins), and Wntless (a sorting receptor for Wnt) (9, 10). Intriguingly, some protein toxins produced by bacteria and plants, e.g., cholera toxin, Shiga toxin, and ricin, highjack this retrograde traffic to reach the cytosol, where they exert their toxicity (11, 12). The retrograde membrane traffic from the PM to the Golgi is known to pass through early endosomes (EEs)/recycling endosomes (REs) (10, 13). The molecular mechanism underlying this traffic has just begun to be elucidated (8, 9).

Here we report that PS is essential for retrograde membrane traffic at REs. PS was most concentrated in REs among intracellular organelles, and evectin-2 (evt-2), a protein of previously unknown function, was targeted to REs by the binding of its pleckstrin homology (PH) domain to PS. Depletion of evt-2 or masking of intracellular PS suppressed membrane traffic from REs to the Golgi. These findings uncover the molecular basis that controls the retrograde transport through REs, and identify a PH domain that specifically recognizes PS.

Results and Discussion

Evectin-1 (evt-1) and -2 are identified as post-Golgi proteins of unknown function (14) that have a PH domain that typically binds polyphosphoinositides (15). Evt-2 is expressed in a broad range of tissues, whereas evt-1 is expressed specifically in the nervous system. We first examined the subcellular localization of evt-2 using COS-1 cells in which organelles are spatially well separated (16, 17) (Fig. S1). Evt-2 colocalized with an RE marker, transferrin receptor (TfnR), but not with a Golgi marker (GM130), a lysosomal marker (LAMP1), or an early endosomal marker (VPS26) (Fig. 1*A*, for quantification see Fig. S2*A*). By immunoelectron microscopy using ultrathin cryosections, GFP–evt-2 (labeled with 10 nm gold particles) was specifically detected in tubulovesicular structures, and TfnR (labeled with 5 nm gold particles) was detected in some of them (Fig. 1*B* and Fig. S3). We thus concluded that evt-2 is localized predominantly to REs.

Author contributions: T.I., R. Kato, S.W., T. Natsume, E.M., N.T., W.I.L., T.T., and H.A. designed research; Y. Uchida, J.H., D.C., S.O., R.M., M.K., S.-i.I., R. Kuwahara, T. Nakagawa, K.N., K.M., D.S., and T.T. performed research; S.-i.I. and T. Natsume contributed new reagents/analytic tools; Y. Uchida, J.H., R.M., and Y. Uchiyama analyzed data; and T.T. and H.A. wrote the paper.

The authors declare no conflict of interest.

*This Direct Submission article had a prearranged editor.

Freely available online through the PNAS open access option.

Data deposition: The coordinates and structure factors have been deposited in the Protein Data Bank, www.pdb.org (PDB ID code 3AJ4).

[1]Y. Uchida and J.H. contributed equally to this work.

[2]To whom correspondence may be addressed. E-mail: tom_taguchi@mol.f.u-tokyo.ac.jp or harai@mol.f.u-tokyo.ac.jp.

This article contains supporting information online at www.pnas.org/lookup/suppl/doi:10.1073/pnas.1109101108/-/DCSupplemental.

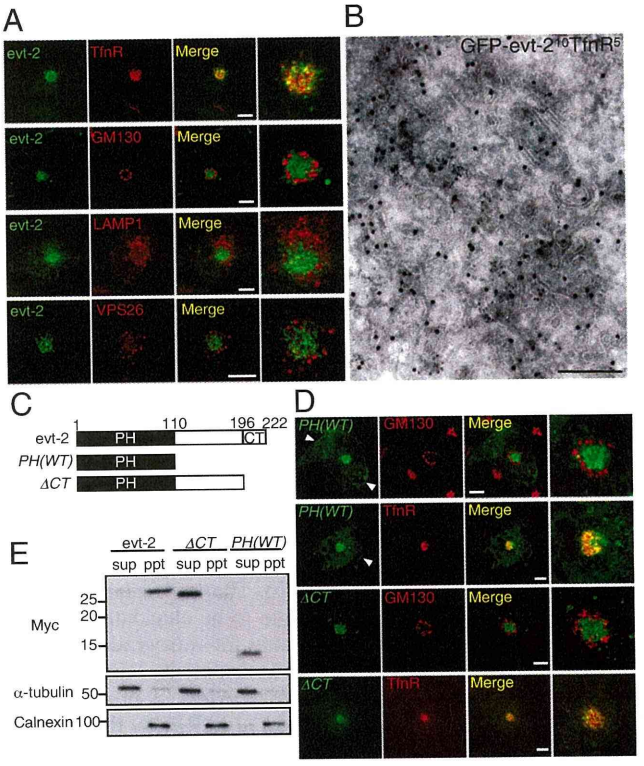

Fig. 1. A PH-domain–containing protein, evt-2, localizes to REs. (*A*) Evt-2 tagged with Myc was transiently expressed in COS-1 cells. The cells were then fixed and stained for Myc, TfnR, GM130, LAMP1, and VPS26. Magnified images around the Golgi/REs region are shown in the *Right* column. (Scale bars, 10 μm.) (*B*) Electron micrograph of an ultrathin cryosection of COS-1 cells. Cells expressing GFP–evt-2 were labeled with antibodies against GFP (10 nm in diameter) and TfnR (5 nm in diameter). (Scale bar, 250 nm.) (*C*) Domain structures of evt-2 and its truncation mutants. Myc-epitope was added to all of the constructs at the N terminus. (*D*) *PH(WT)* and *ΔCT* were transiently expressed. The cells were then fixed and stained for Myc, GM130, and TfnR. Arrowheads indicate PM. (Scale bars, 10 μm.) (*E*) Evt-2, *ΔCT*, and *PH(WT)* were transiently expressed in COS-1 cells for 24 h. Cell lysates were spun at 100,000 *g* for 60 min at 4 °C, and the resultant supernatant (sup) and pellet (ppt) were immunoblotted with anti-Myc antibody. α-Tubulin and calnexin were immunoblotted as a control.

Evt-2 also colocalized with the RE marker TfnR in HeLa cells (Fig. S4*A*).

Evt-2 has an N-terminal PH domain and a C-terminal hydrophobic region (CT) (Fig. 1*C*). *PH(WT)*, a Myc-tagged evt-2 PH domain, was targeted to REs and to the PM to some extent (Fig. 1*D*). The PH domain is thus sufficient for evt-2 targeting to REs. *ΔCT* was exclusively localized to REs as evt-2, suggesting that the domain between PH and CT constrains the RE localization of evt-2. Evt-2 was recovered in the pellet after ultracentrifugation of cell lysate, whereas truncation mutants (*ΔCT* and *PH(WT)*) were found in the supernatant (Fig. 1*E*), showing that CT is required for evt-2 association with membranes.

The human proteome has ~300 proteins with PH domains. About 10% of these proteins bind specifically to phosphatidylinositol phosphates (PIPs) through their PH domains, whereas the ligands of the rest of these proteins remain unclear (15). To determine the lipid specificity of evt-2 PH, we measured the binding of several negatively charged lipids on liposomes to recombinant evt-2 PH. Unexpectedly, PS bound to the PH, but phosphatidic acid, phosphatidylinositol, sulfatide, and all PIPs did not (Fig. 2 *A* and *B*). Lys20 is highly conserved in other PH domains (18). Evt-2 PH (K20E) lost the ability to bind to PS.

A *Saccharomyces cerevisiae* mutant (*cho1*Δ) deficient in PS (19, 20) is used to analyze protein binding to PS in vivo (4, 5). We expressed evt-2 PH in wild-type yeast and found that it was not associated with the PM. Because a tandem fusion of lipid-binding modules, such as the FYVE domain of EEA1 and Hrs, greatly enhances the lipid-binding affinity of the FYVE domain (21), we generated a tandem evt-2 PH (*2 × PH*) and expressed it in both the wild-type and *cho1*Δ mutant. *2 × PH* was observed predominantly on the PM of the wild-type yeast, whereas it was cytosolic in the PS-deficient mutant (Fig. 2*C*). The C2 domain of lactadherin (Lact-C2), a specific probe for PS (4), was used as a positive control. These findings showed that evt-2 PH recognizes PS in vivo.

Several intracellular organelles possess unique phospholipids such as PIPs, although the specific phospholipids in REs are not well characterized (22). We therefore expressed a variety of phospholipid probes in cells to see their distribution. None of the PIP probes stained REs (Fig. S5), but Lact-C2 predominantly stained REs and the PM (Fig. 2*D*, for quantification see Fig. S2*B*), revealing that REs are most enriched with PS among intracellular organelles. The enrichment of PS in REs was also confirmed in HeLa cells (Fig. S4*B*). Given the ligand specificity of the evt-2 PH, the binding of evt-2 PH to PS is likely to be involved in evt-2 localization to REs.

We were able to grow crystals of human evt-2 PH (a recombinant 110-amino acid domain) in complex with O-phospho-L-serine, the head group of PS, and analyzed them by X-ray crystallography at 1.0 Å resolution. The data collection and refinement statistics are summarized in Table S1. The overall structure was similar to the standard PH domain fold, with seven β strands forming two orthogonal antiparallel β sheets and two α helices containing the major C-terminal α helix (Fig. 3*A*). O-phospho-L-serine binds to the positively charged pocket made by three basic residues (Arg11, Arg18, and Lys20) and the backbone nitrogen atoms of three residues (Thr14, Ile15, and Leu16) of the β1/β2 loop (Fig. 3 *B* and *C* and Table S2). Arg11 and Arg18 each make two salt bridges with the L-serine oxygen atoms and the phosphate oxygen of the ligand, respectively (Fig. 3*B* and Table S2). In addition, Lys20 makes salt bridges with both moieties of the ligand. The nitrogen atom of O-phospho-L-serine forms a salt bridge with the side chain of Glu44 in one of the two conformers in the crystal (Fig. S6*A*).

We next examined whether the amino acid residues involved in the ligand binding in the crystal are essential for evt-2 localization to REs. The full-length point mutant *K20E*, in which Lys20 was changed to Glu, lost RE localization and showed puncta around the Golgi (Fig. 4*A*, for quantification see Fig. S2*A*). These puncta did not colocalize with TfnR (REs), but colocalized in part with VPS26 (EEs) and CD63 (late endosomes,LEs). The PH point mutant of Arg11, Arg18, or Lys20 (*PH(R11E)*, *PH(R18E)*, and *PH(K20E)*) did not show any specific membrane localization (Fig. 4*B*), suggesting that these residues bind to the head group of PS in vivo. All of the residues involved in the direct interaction of the ligand (Table S2) were conserved in the evt-2 PH of other species (Fig. 4*C*), further implicating these residues in the recognition of PS.

Two membrane trafficking pathways pass through REs: one is a recycling pathway and the other is a retrograde pathway that links the PM to the Golgi/ER (10). We examined whether evt-2 is involved in these pathways. Evt-2 knockdown did not cause any gross change in Tfn recycling to the PM (Fig. S7 *A* and *B*). Cholera toxin travels from the PM through endosomes (EEs/REs) to the Golgi/ER, and is finally translocated into the cytosol (11). Alexa 594-labeled cholera toxin B subunit (CTxB) was pulsed for 5 min and chased (Fig. 5*A*). After a 5-min uptake, CTxB accumulated around the Golgi, colocalizing in part with VPS26, showing that it reached EEs (Fig. S8*A*). After a 15-min pulse/chase, CTxB accumulated at the cell center, colocalizing with Tfn, showing it reached REs (Fig. S8*B*). After a 60–90 min pulse/chase, CTxB showed a good

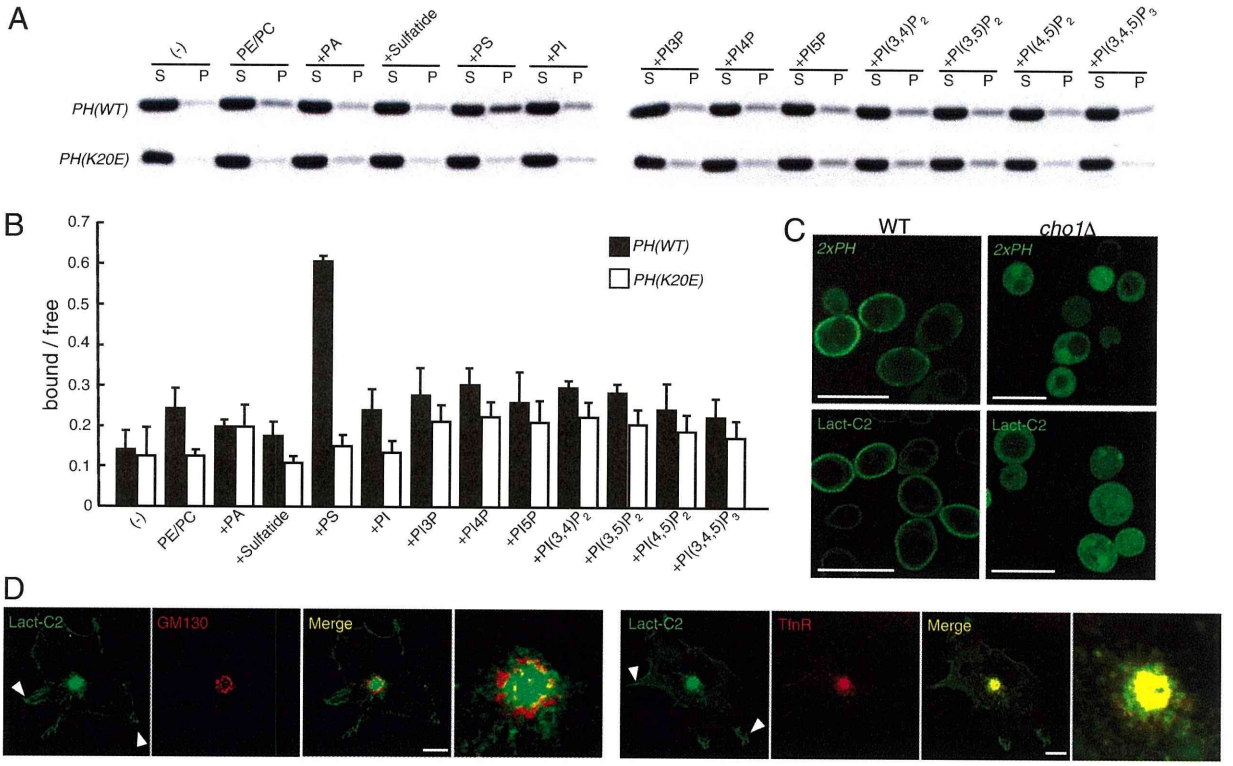

Fig. 2. Evt-2 PH binds to PS. (*A* and *B*) His-tagged evt-2 PH (WT or K20E) was mixed with liposomes harboring the indicated negatively charged lipid (20% mol/mol of total lipids). After 15 min, the mixture was spun at 100,000 *g* for 30 min, and the resultant supernatant (S) and pellet (P) were subjected to SDS-PAGE. The gels were stained with Coomassie blue (*A*). The intensities of individual bands were quantitated with NIH ImageJ. The values of "P (bound)/S (free)" are shown in a bar graph (*B*). Data represent mean values ± SD of three independent experiments. PE, phosphatidylethanolamine; PC, phosphatidylcholine; PA, phosphatidic acid; PI, phosphatidylinositol. (*C*) Confocal images of wild-type yeast cells and *cho1*Δ cells expressing GFP-tagged *2 × PH* (a tandem fusion of evt-2 PH) or GFP–Lact-C2. (Scale bars, 10 μm.) (*D*) COS-1 cells were transfected with GFP–Lact-C2, then fixed, and stained for GM130 or TfnR. Arrowheads indicate PM. (Scale bars, 10 μm.)

colocalization with GM130. These results showed the sequential retrograde transport of CTxB from the PM to the Golgi through EEs and then REs. In cells depleted of evt-2 by using siRNA 1 (Fig. 5*B*), CTxB transport to REs proceeded normally after a 15-min pulse/chase, but CTxB transport from REs to the Golgi was significantly impaired after a 60- or 90-min pulse/chase. The other siRNA oligos 2 and 3 also impaired CTxB traffic to the Golgi (Fig. S7*C*, for quantification see *D*). Thus, evt-2 is required for retrograde transport of CTxB from REs to the Golgi.

The effect of evt-2 knockdown on retrograde transport was also examined by biochemical assays using a mutant CTxB (CTxB-GS) harboring tyrosine sulfation and N-glycosylation sites to monitor its arrival at the Golgi or ER (23), and using cholera toxin to measure the increase of intracellular cAMP that occurs when the toxin

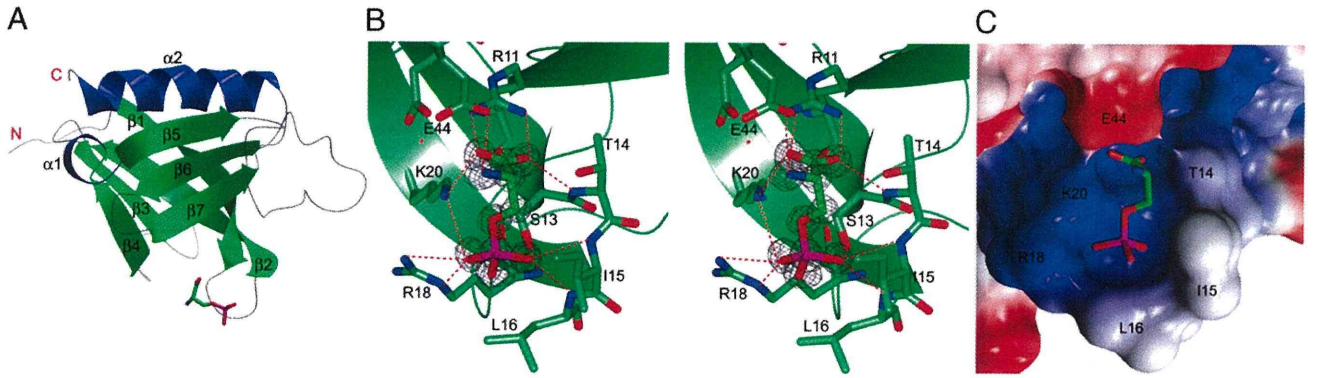

Fig. 3. High-resolution structure of evt-2 PH bound to phosphoserine. (*A*) Overall structure of human evt-2 PH in complex with O-phospho-L-serine, consisting of seven β strands and two helices. The amino and carboxy termini are denoted in red as N and C, respectively. O-phospho-L-serine is shown as a stick model. (*B*) Stereoview of the O-phospho-L-serine binding site of evt-2 PH. Interacting residues are shown as stick models. A σA-weighted *Fo-Fc* omit map (3.0 σ level; in gray mesh) is superposed on O-phospho-L-serine. Hydrogen bonds and salt bridges are shown as red broken lines. (*C*) Charge distribution surface model of evt-2 PH in complex with O-phospho-L-serine (stick model). The surface is colored according to the electrostatic potential of the residues (blue, positive; red, negative). Only one of the double conformers of Glu44 is shown.

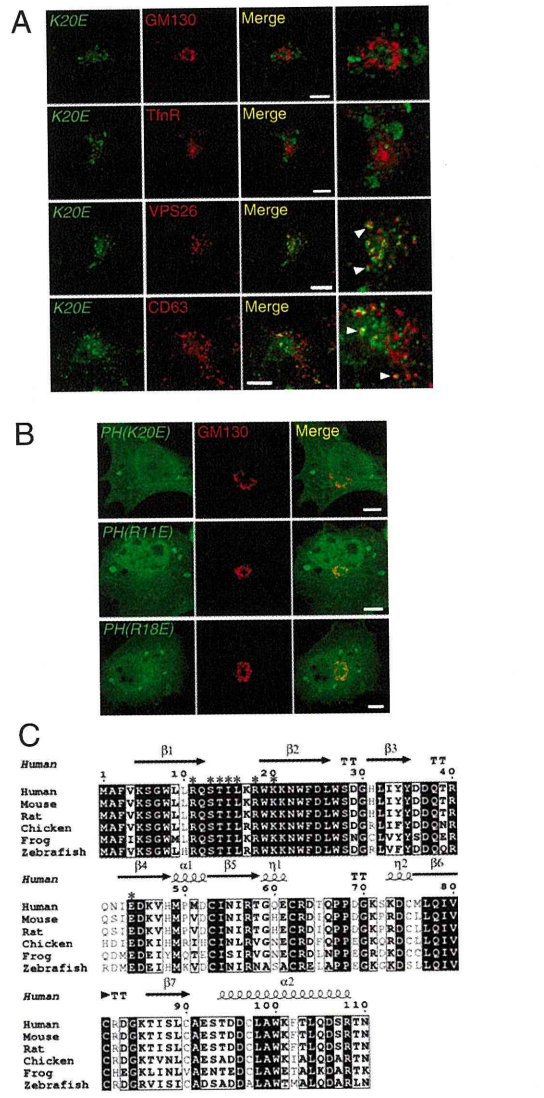

Fig. 4. The amino acid residues involved in the ligand binding in the crystal are essential for evt-2 localization to REs. (*A*) The full-length point mutant *K20E*, in which Lys20 was changed to Glu, was transiently expressed in COS-1 cells. The cells were then fixed and stained for Myc, GM130, TfnR, VPS26, and CD63. Arrowheads indicate puncta where *K20E* and endosomal markers are juxtaposed or colocalized. (Scale bars, 10 μm.) (*B*) The PH point mutants *PH (K20E)*, *PH(R11E)*, and *PH(R18E)*, in which Lys20, Arg11, or Arg18 was changed to Glu, were transiently expressed. The cells were then fixed and stained for Myc and GM130. (Scale bars, 10 μm.) (*C*) Alignment of vertebrate evt-2 PH domains. The secondary structure elements of human evt-2 PH are shown above the sequence. Conserved residues are boxed in white on a black background. Similar residues are boxed in black with a white background. Asterisks indicate the residues directly involved in the interaction of the ligand.

arrives in the cytosol. Both assays confirmed the impaired retrograde traffic of cholera toxin upon depletion of evt-2 (Fig. 5 *C* and *D* and Fig. S7*E*).

Evt-2 depletion did not significantly alter the subcellular localizations of a Golgi marker (GM130), a lysosomal marker (LAMP2), LE markers [CD63 and cation-independent mannose 6-phosphate receptor (CI-MPR)], or an RE marker (TfnR) (Fig. S7*F*). However, Golgi proteins TGN46 and GP73 no longer localized to the Golgi, but localized on punctate structures upon evt-2 depletion (Fig. 5*E*, for quantification see Fig. S2*C*). These two proteins are known to circulate between the Golgi and the PM through endosomes (10, 24). When retrograde transport from REs to the Golgi is impaired by depletion of evt-2, TGN46 and GP73 may be shunted to circulate among PM, EEs, and REs, resulting in their puncta localization.

Next, we performed knockdown/rescue experiments. Cells were depleted of evt-2 with siRNA 1 and transfected with an siRNA-resistant evt-2 construct (a mouse evt-2 WT or K20E mutant defective in PS binding). Golgi localization of TGN46 was restored in the cells transfected with mouse evt-2 WT (Fig. 5*F*). In contrast, TGN46 remained scattered throughout the cytosol in the cells transfected with evt-2 K20E mutant. Therefore, the binding of evt-2 PH to PS is essential for evt-2 function in endosomal membrane trafficking.

We further examined how blocking PS would affect endosomal membrane transport. Lact-C2 was overexpressed to mask PS in the cytosolic leaflet of REs. CTxB transport to the Golgi was severely delayed and accumulated in REs in the cells transfected with Lact-C2 (Fig. 5*G*, for quantification see Fig. S2*D*), showing that exposure of PS in the cytosolic surface of REs is required for CTxB transport from REs to the Golgi.

Recent studies in yeast and mammalian cells have established that the retromer complex at EEs has a critical function in retrograde membrane traffic to the Golgi (8, 25). In this study, besides EEs, we showed that REs are involved in this membrane traffic for certain cargo proteins. Retrograde and recycling traffickings diverge at REs, with a previously uncharacterized PH-domain–containing protein evt-2, which is essential and specific for retrograde traffic. We found that GP73, which circulates between the Golgi and the PM through endosomes, binds to evt-2 (Fig. S9). Together with the fact that evt-2 depletion abolished GP73 localization at the Golgi (Fig. 5*E*), we assume that evt-2 functions as a sorting device at REs to recruit specific cargo molecules that follow retrograde transport to the Golgi. We and other groups have shown that REs also play an obligatory role in the exocytic pathway for various secretory cargos (17, 26, 27). REs, therefore, can handle three membrane trafficking pathways: the recycling pathway (EEs → REs → PM), the exocytic pathway (the Golgi → REs → PM), and the retrograde pathway (EEs → REs → the Golgi).

The PH domain in evt-2 specifically binds PS, but not PIPs. What is the structural basis underlying the specificity of evt-2 PH to PS? All high-affinity, stereospecific PH domains for PIPs share a similar binding site (15). The β1/β2 loop functions as a platform for the interaction with the head group of the ligand. This loop lines a deep binding pocket and contains the sequence motif $KX_n(K/R)XR$ (where X is any amino acid), in which the basic side chains participate in most phosphate-group interactions. The corresponding motif in evt-2 PH is $R^{11}X_nK^{20}XN$, where italics indicate changes, and of note, the two nitrogen atoms (Nη1 and Nη2) of Arg11 make two salt bridges neatly with the carboxyl group of O-phospho-L-serine, which is absent in PIPs. A search for 3D structures homologous to human evt-2 PH using the DALI server (28) yielded the DAPP1/PHISH PH domain in complex with $Ins(1,3,4,5)P_4$ (Protein Data Bank code, 1FAO) as the best match (29). A comparison of the structures of the two complexes suggests that some evt-2 PH amino acids would clash with the head group of $Ins(1,3,4,5)P_4$ (Fig. S6 *B* and *C*). Thr14, Ile15, and Leu16 of evt-2 PH are close to the ligand, and the ligand-binding site is much smaller than that of DAPP1 PH. Therefore, the tightness of the ligand-binding site might account for the specificity of evt-2 PH for PS. Several simultaneous recognitions were identified in evt-2 PH (Fig. 3*B* and Table S2). Among them, Lys20 and Ile15 appear particularly important because they recognize both the L-serine and phosphate regions of the ligand. Simultaneous recognition of multiple regions of a ligand by interacting residues might enhance the binding affinity and specificity.

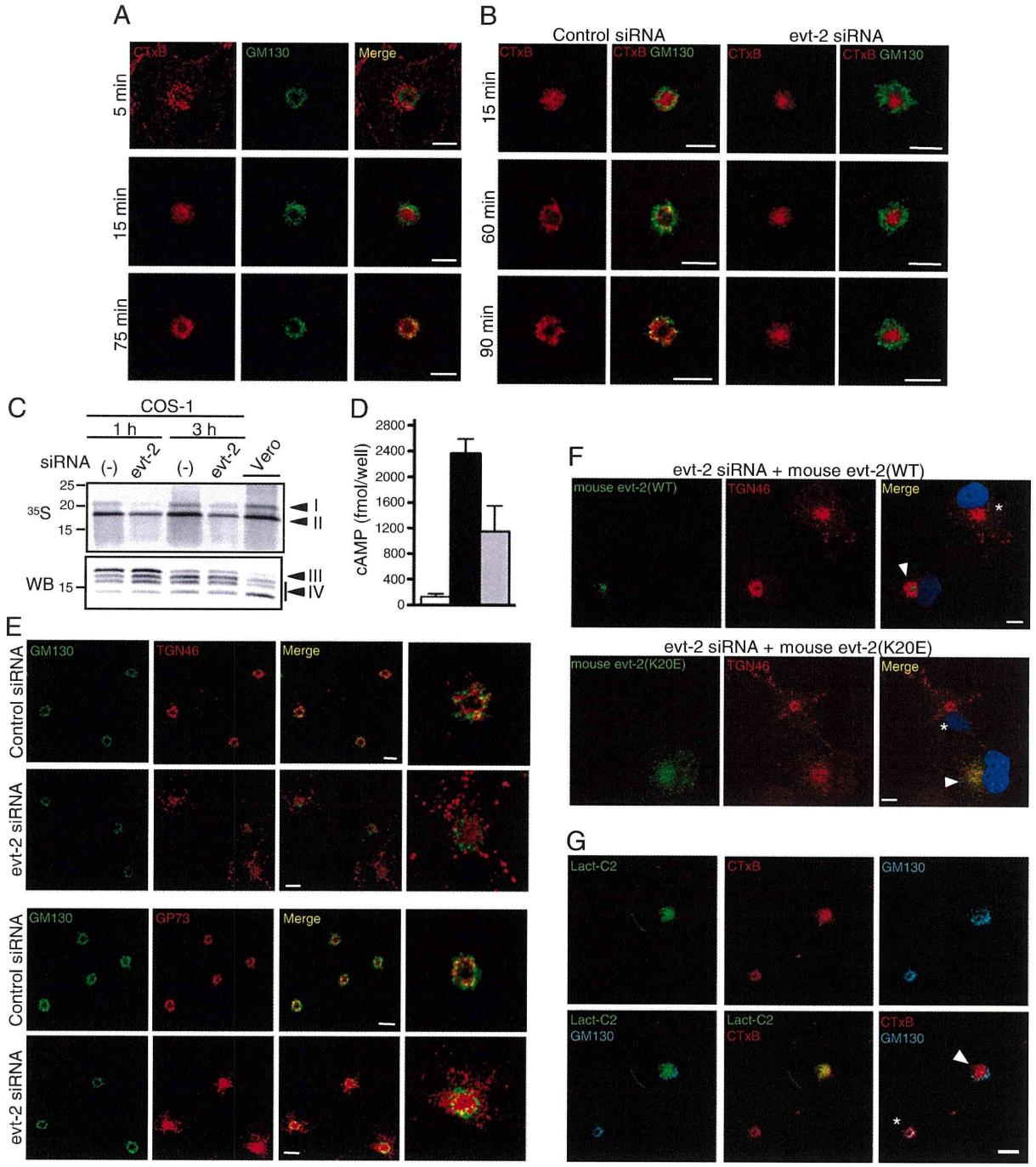

Fig. 5. Evt-2 and PS regulate retrograde transport through REs. (*A*) COS-1 cells were pulsed for 5 min at 37 °C with Alexa 594-CTxB and chased. Cells were then fixed at the indicated times from the beginning of the pulse, and stained for GM130. (Scale bars, 10 μm.) (*B*) Cells were treated with evt-2 siRNA 1 or control siRNA for 48 h. The pulse/chase of CTxB was performed as described in *A*. (Scale bars, 10 μm.) (*C*) Cells were treated with evt-2 siRNA 1 or mock treated for 48 h. Cells were then incubated with ^{35}S and CTxB-GS at 37 °C. CTxB-GS was immunoprecipitated and analyzed by autoradiography (*Upper*). A parallel experiment on Vero cells was carried out as control. The *Lower* band (II) represents the sulfated, but nonglycosylated CTxB. The *Upper* band (I) is N glycosylated. Thus, CTxB traveled from the PM to the Golgi and a significant fraction of the Golgi-modified protein moved to the ER. In cells depleted of evt-2, the intensity of ^{35}S-labeling of CTxB at both 1 and 3 h was reduced by 62–68%. In contrast, transport of CTxB beyond the Golgi to the ER was not affected (about 10% of the sulfated CTxB was glycosylated in both conditions). (*Lower*) Immunoblot (WB) of samples using an antibody against CTxB as loading control for autoradiogram. *Top* band (III) shows CTxB-GS. Bands labeled IV are degradation products. (*D*) Cells were treated with either evt-2 siRNA 1 or transfection reagent only for 48 h. Following addition of 1 nM cholera toxin, intracellular cAMP levels were measured at 50-min time point: evt-2 siRNA-treated cells (gray column), control cells (transfection reagent only, black column), and the cells without cholera toxin addition (white column). Data represent mean values of three independent experiments. (*E*) Cells treated with either evt-2 siRNA 1 or control siRNA were fixed and costained for GM130/TGN46 or GP73/GM130. Magnified images around the Golgi/REs region in one of the cells for each condition are shown in the *Right* column. (Scale bars, 10 μm.) (*F*) Cells were cotransfected with evt-2 siRNA 1 and siRNA-resistant mouse evt-2 constructs tagged with Myc (WT or K20E). After 72 h, cells were fixed and costained for Myc/TGN46. Arrowheads indicate cells expressing evt-2, and asterisks indicate nonexpressing cells. (Scale bars, 10 μm.) (*G*) Transient expression of GFP–Lact-C2. Cells were pulsed for 5 min with Alexa 594-CTxB, chased, fixed at 60 min after the beginning of the pulse, and stained for GM130. The arrowhead indicates a cell expressing GFP–Lact-C2, and the asterisk indicates a nonexpressing cell. (Scale bar, 10 μm.)

In this study, we showed that PS recognition by the PH domain of evt-2 is essential for endosomal membrane transport from the PM to the Golgi. The data presented here provide compelling evidence that intracellular PS has a critical role in membrane traffic and uncover the molecular basis that controls the RE-to-Golgi transport.

Materials and Methods

Cell Culture and Transfection. COS-1 cells were cultured at 37 °C with 5% CO_2 in DMEM containing 10% heat-inactivated FCS. Transfection was performed using Lipofectamine 2000 (Invitrogen) according to the manufacturer's instructions.

Structure Determination. The complex structure of human evt-2 PH with O-phospho-L-serine was determined by the molecular replacement method at 1.0 Å resolution using the data collected at beamline AR-NW12A of the Photon Factory. The crystal belongs to space group $P2_1$, with a = 31.7 Å, b = 48.4 Å, c = 64.3 Å, and β = 92.2°. The coordinates and structure factors of the human evt-2 PH structure have been deposited in the Protein Data Bank with the accession code 3AJ4.

Additional materials and methods are provided in *SI Materials and Methods*.

ACKNOWLEDGMENTS. A special thanks to Wendy Hamman for help with tissue culture and transfection conditions. This work was supported by the Core Research for Evolutional Science and Technology, Japan Science and Technology Agency (H.A. and T.T.), the Program for Promotion of Basic and Applied Research for Innovations in Bio-Oriented Industry (H.A.), the 21st Century Center of Excellence Program from the Ministry of Education, Culture, Sports, Science, and Technology of Japan (T.T.), Grants-in-aid for Scientific Research (20370045 to H.A. and 18050019 to T.T.), and a Senri Life Science Foundation Grant (to T.T.).

1. Leventis PA, Grinstein S (2010) The distribution and function of phosphatidylserine in cellular membranes. *Annu Rev Biophys* 39:407–427.
2. Huang M, et al. (2003) Structural basis of membrane binding by Gla domains of vitamin K-dependent proteins. *Nat Struct Biol* 10:751–756.
3. Verdaguer N, Corbalan-Garcia S, Ochoa WF, Fita I, Gómez-Fernández JC (1999) Ca(2+) bridges the C2 membrane-binding domain of protein kinase Calpha directly to phosphatidylserine. *EMBO J* 18:6329–6338.
4. Yeung T, et al. (2008) Membrane phosphatidylserine regulates surface charge and protein localization. *Science* 319:210–213.
5. Moravcevic K, et al. (2010) Kinase associated-1 domains drive MARK/PAR1 kinases to membrane targets by binding acidic phospholipids. *Cell* 143:966–977.
6. Gagescu R, et al. (2000) The recycling endosome of Madin-Darby canine kidney cells is a mildly acidic compartment rich in raft components. *Mol Biol Cell* 11:2775–2791.
7. Mellman I, Warren G (2000) The road taken: Past and future foundations of membrane traffic. *Cell* 100:99–112.
8. Bonifacino JS, Rojas R (2006) Retrograde transport from endosomes to the trans-Golgi network. *Nat Rev Mol Cell Biol* 7:568–579.
9. Johannes L, Popoff V (2008) Tracing the retrograde route in protein trafficking. *Cell* 135:1175–1187.
10. Maxfield FR, McGraw TE (2004) Endocytic recycling. *Nat Rev Mol Cell Biol* 5:121–132.
11. Lencer WI, Tsai B (2003) The intracellular voyage of cholera toxin: Going retro. *Trends Biochem Sci* 28:639–645.
12. Sandvig K, van Deurs B (2002) Membrane traffic exploited by protein toxins. *Annu Rev Cell Dev Biol* 18:1–24.
13. Mallard F, et al. (1998) Direct pathway from early/recycling endosomes to the Golgi apparatus revealed through the study of shiga toxin B-fragment transport. *J Cell Biol* 143:973–990.
14. Krappa R, Nguyen A, Burrola P, Deretic D, Lemke G (1999) Evectins: Vesicular proteins that carry a pleckstrin homology domain and localize to post-Golgi membranes. *Proc Natl Acad Sci USA* 96:4633–4638.
15. Lemmon MA (2008) Membrane recognition by phospholipid-binding domains. *Nat Rev Mol Cell Biol* 9:99–111.
16. Misaki R, Nakagawa T, Fukuda M, Taniguchi N, Taguchi T (2007) Spatial segregation of degradation- and recycling-trafficking pathways in COS-1 cells. *Biochem Biophys Res Commun* 360:580–585.
17. Misaki R, et al. (2010) Palmitoylated Ras proteins traffic through recycling endosomes to the plasma membrane during exocytosis. *J Cell Biol* 191:23–29.
18. Dowler S, et al. (2000) Identification of pleckstrin-homology-domain-containing proteins with novel phosphoinositide-binding specificities. *Biochem J* 351:19–31.
19. Atkinson KD, et al. (1980) Yeast mutants auxotrophic for choline or ethanolamine. *J Bacteriol* 141:558–564.
20. Hikiji T, Miura K, Kiyono K, Shibuya I, Ohta A (1988) Disruption of the CHO1 gene encoding phosphatidylserine synthase in Saccharomyces cerevisiae. *J Biochem* 104: 894–900.
21. Gillooly DJ, et al. (2000) Localization of phosphatidylinositol 3-phosphate in yeast and mammalian cells. *EMBO J* 19:4577–4588.
22. Di Paolo G, De Camilli P (2006) Phosphoinositides in cell regulation and membrane dynamics. *Nature* 443:651–657.
23. Fujinaga Y, et al. (2003) Gangliosides that associate with lipid rafts mediate transport of cholera and related toxins from the plasma membrane to endoplasmic reticulm. *Mol Biol Cell* 14:4783–4793.
24. Puri S, Bachert C, Fimmel CJ, Linstedt AD (2002) Cycling of early Golgi proteins via the cell surface and endosomes upon lumenal pH disruption. *Traffic* 3:641–653.
25. Seaman MN, McCaffery JM, Emr SD (1998) A membrane coat complex essential for endosome-to-Golgi retrograde transport in yeast. *J Cell Biol* 142:665–681.
26. Ang AL, et al. (2004) Recycling endosomes can serve as intermediates during transport from the Golgi to the plasma membrane of MDCK cells. *J Cell Biol* 167:531–543.
27. Murray RZ, Kay JG, Sangermani DG, Stow JL (2005) A role for the phagosome in cytokine secretion. *Science* 310:1492–1495.
28. Holm L, Sander C (1995) Dali: A network tool for protein structure comparison. *Trends Biochem Sci* 20:478–480.
29. Ferguson KM, et al. (2000) Structural basis for discrimination of 3-phosphoinositides by pleckstrin homology domains. *Mol Cell* 6:373–384.